

Charm Mass Determination from QCD Charmonium Sum Rules at Order α_s^3

Bahman Dehnadi^{a,b} Andre H. Hoang^{b,c} Vicent Mateu,^{c,d,e,1} S. Mohammad Zebarjad^a

^a*Shiraz University, Physics Department, Shiraz 71454, Iran.*

^b*University of Vienna, Faculty of Physics, Boltzmanngasse 5, A-1090 Vienna, Austria.*

^c*Max-Planck-Institut für Physik (Werner-Heisenberg-Institut), Föhringer Ring 6, D-80805 München, Germany.*

^d*Center for Theoretical Physics, Massachusetts Institute of Technology, Cambridge, MA 02139.*

^e*Instituto de Física Corpuscular, Universitat de València – Consejo Superior de Investigaciones Científicas, Parc Científic, E-46980 Paterna (Valencia), Spain.*

E-mail: bahman.dehnadi@univie.ac.at, andre.hoang@univie.ac.at,
mateu@ific.uv.es, zebarjad@susc.ac.ir

ABSTRACT: We determine the $\overline{\text{MS}}$ charm quark mass from a charmonium QCD sum rules analysis. On the theoretical side we use input from perturbation theory at $\mathcal{O}(\alpha_s^3)$. Improvements with respect to previous $\mathcal{O}(\alpha_s^3)$ analyses include (1) an account of all available e^+e^- hadronic cross section data and (2) a thorough analysis of perturbative uncertainties. Using a data clustering method to combine hadronic cross section data sets from different measurements we demonstrate that using all available experimental data up to c.m. energies of 10.538 GeV allows for determinations of experimental moments and their correlations with small errors and that there is no need to rely on theoretical input above the charmonium resonances. We also show that good convergence properties of the perturbative series for the theoretical sum rule moments need to be considered with some care when extracting the charm mass and demonstrate how to set up a suitable set of scale variations to obtain a proper estimate of the perturbative uncertainty. As the final outcome of our analysis we obtain $\overline{m}_c(\overline{m}_c) = 1.282 \pm (0.006)_{\text{stat}} \pm (0.009)_{\text{syst}} \pm (0.019)_{\text{pert}} \pm (0.010)_{\alpha_s} \pm (0.002)_{\langle GG \rangle}$ GeV. The perturbative error is an order of magnitude larger than the one obtained in previous $\mathcal{O}(\alpha_s^3)$ sum rule analyses.

KEYWORDS: QCD, perturbative corrections

¹Corresponding author.

Contents

1	Introduction	1
2	Theoretical Input	4
2.1	Perturbative Contribution	4
2.2	Gluon Condensate Contribution	10
2.3	Running Coupling and Mass	11
2.4	Perturbative Uncertainties in the $\overline{\text{MS}}$ Charm Mass	12
3	Experimental Data	17
3.1	Data Collections	17
3.2	Data Combination	23
3.3	Experimental Moments	27
3.4	Examination	33
4	Charm Quark Mass Analysis for the First Moment	35
5	Higher Moment Analysis	37
6	Conclusions and Final Thoughts	40
	Appendix A: Results of the Fit Procedure	43
	Appendix B: On the Equivalence of χ^2-Functions	44
	Appendix C: Dependence on α_s for Higher Moment Analyses	50

1 Introduction

Accurate determinations of the charm quark mass are an important ingredient in the prediction of inclusive and radiative B decays or exclusive kaon decays such as $K \rightarrow \pi\nu\bar{\nu}$. Since these decays are instruments to either measure CKM matrix elements or to search for new physics effects, appropriate and realistic estimates of the uncertainties are also an important element of these analyses [1].

One of the most powerful methods to determine the charm quark mass is based on sum rules for the charm-anticharm production rate in e^+e^- annihilation [2]. Here, moments of

the correlation function of two charm vector currents at zero momentum transfer

$$\begin{aligned}
M_n^{\text{th}} &= \frac{12\pi^2 Q_c^2}{n!} \frac{d}{dq^{2n}} \Pi(q^2) \Big|_{q^2=0}, \\
(g_{\mu\nu} q^2 - q_\mu q_\nu) \Pi(q^2) &= -i \int dx e^{iqx} \langle 0 | T j_\mu(x) j_\nu(0) | 0 \rangle, \\
j^\mu(x) &= \bar{\psi}(x) \gamma^\mu \psi(x),
\end{aligned} \tag{1.1}$$

Q_c being the charm quark electric charge, can be related to weighted integrals of the normalized charm cross section

$$\begin{aligned}
M_n &= \int \frac{ds}{s^{n+1}} R_{e^+e^- \rightarrow c\bar{c}+X}(s), \\
R_{e^+e^- \rightarrow c\bar{c}+X}(s) &= \frac{\sigma_{e^+e^- \rightarrow c\bar{c}+X}(s)}{\sigma_{e^+e^- \rightarrow \mu^+\mu^-}(s)},
\end{aligned} \tag{1.2}$$

which can be obtained from experiments. For small values of n such that $m_c/n \gtrsim \Lambda_{\text{QCD}}$ the theoretical moments M_n^{th} can be computed in an operator product expansion (OPE) where the dominant part is provided by perturbative QCD supplemented by small vacuum condensates that parametrize nonperturbative effects [3, 4]. The leading gluon condensate power correction term has a surprisingly small numerical effect and is essentially negligible for the numerical analysis as long as n is small.

This allows to determine the charm mass in a short distance scheme such as $\overline{\text{MS}}$ to high precision [5]. This method to determine the $\overline{\text{MS}}$ charm mass is frequently called charmonium sum rules. For the theoretical moments the perturbative part of the OPE is known at $\mathcal{O}(\alpha_s^0)$ and $\mathcal{O}(\alpha_s)$ for any value of n [6]. At $\mathcal{O}(\alpha_s^2)$ the moments are known to high values of n [7–11], and to $\mathcal{O}(\alpha_s^3)$ for $n = 1$ [12, 13], $n = 2$ [14], and $n = 3$ [15]. Higher moments at $\mathcal{O}(\alpha_s^3)$ have been determined by a semianalytical procedure [16, 17] (see also [18]). The Wilson coefficient of the gluon condensate contribution is known to $\mathcal{O}(\alpha_s)$ [19]. On the experimental side the total hadronic cross section in e^+e^- annihilation is known from various experimental measurements for c.m. energies up to 10.538 GeV. None of the experimental analyses actually ranges over the entire energy region between the charmonium region and 10.538 GeV, but different analyses overlapping in energy exist such that energies up to 10.538 GeV are completely covered [20–37].¹ Interestingly, to the best of our knowledge, the complete set of all available experimental data on the hadronic cross section has never been used in previous charmonium sum rule analyses to determine the experimental moments. Rather, sum rule analyses have relied heavily on theoretical input using different approaches to determine the corresponding “experimental error” and intrinsically leading to a sizable modeling uncertainty for energy regions below 10.538 GeV for low values of n [38].

¹As a word of caution we mention that, except for the contributions of the J/ψ and ψ' resonances, no experimental separation of the charm and non-charm contributions in the hadronic cross section has been provided in available data, although charm-tagged measurements are possible, see e.g. Ref. [31] (CLEO collaboration). So the charm pair production rate from above the J/ψ and ψ' that enters the charmonium sum rules in Eq. (1.2) is usually obtained partly from the measured total R -ratio with theory motivated subtractions of the non-charm rate, and partly by using theory predictions for the charm production rate.

The most recent charmonium sum rule analysis based on Eqs. (1.1) and (1.2), carried out by Kühn et al. [39, 40]² using input from perturbative QCD (pQCD) at $\mathcal{O}(\alpha_s^3)$ for the perturbative contribution, obtained $\bar{m}_c(\bar{m}_c) = 1279 \pm (2)_{\text{pert}} \pm (9)_{\text{exp}} \pm (9)_{\alpha_s} \pm (1)_{\langle \text{GG} \rangle}$ MeV where the first quoted error is the perturbative uncertainty and the second is the experimental one. The third and the fourth quoted uncertainties come from α_s and the gluon condensate correction, respectively.³ To our knowledge this result, the outcome of similar analyses in Ref. [12] and by Boughezal, Czakon and Schutzmeier [13]⁴, a closely related analysis based on lattice results instead of data for pseudoscalar moments [42, 43], and the finite-energy sum rules analysis by Bodenstein et al. [44] represent the analyses with the highest precision achieved so far in the literature. If confirmed, any further investigations and attempts concerning a more precise charm quark $\overline{\text{MS}}$ mass would likely be irrelevant for any foreseeable future.

We therefore find it warranted to reexamine the charmonium sum rule analysis with special attention on the way how perturbative and experimental uncertainties have been treated in Refs. [39, 40]. A closer look into their analysis reveals that the quoted perturbative uncertainty results from a specific way to arrange the α_s expansion for the charm mass extractions and, in addition, by setting the $\overline{\text{MS}}$ renormalization scales in α_s and in the charm mass (which we call μ_α and μ_m , respectively) equal to each other (i.e., they use $\mu_\alpha = \mu_m$). Moreover, concerning the experimental moments, only data up to $\sqrt{s} = 4.8$ GeV from the BES experiments [21, 24] were used, while for $\sqrt{s} > 4.8$ GeV perturbative QCD predictions were employed. Conceptually this approach is somewhat related to the method of finite energy sum rules (see e.g. Ref. [45]), which we, however, do not discuss in this work. While this approach might be justified to estimate the overall nominal contribution for the experimental moments from $\sqrt{s} > 4.8$ GeV, since perturbative QCD predictions describe quite well the measured total hadronic cross section outside the resonance regions, it is not obvious how this method can provide an experimental uncertainty. Since the region $\sqrt{s} > 4.8$ GeV constitutes about 30% of the first moment M_1 , which is theoretically most reliable, this approach contains a significant intrinsic model dependence that cannot be quantified unambiguously.

In this work we reexamine the charmonium sum rules analysis for low values of n using the latest $\mathcal{O}(\alpha_s^3)$ perturbative results, and we implement improvements which concern the two issues just mentioned:

1. We analyze several different types of perturbative expansions and examine in detail how the result for the $\overline{\text{MS}}$ charm mass depends on independent choices of μ_α and μ_m . We show in particular that the interplay of certain choices for the perturbative expansion and the scale setting $\mu_\alpha = \mu_m$ used in previous $\mathcal{O}(\alpha_s^3)$ analyses leads to sizable cancellations of the dependence on μ_α and μ_m that in the light of our

²Ref. [39] is actually Chetyrkin et al.

³In Refs. [39, 40] the main quoted result is for $\bar{m}_c(3\text{GeV})$. For $\bar{m}_c(\bar{m}_c)$ the central value and total errors are quoted. We have extracted the individual errors from results in their paper.

⁴Since the analyses of Refs. [12, 13] were based on outdated and less precise data for the J/ψ and ψ' electronic partial widths [41], we frequently only compare our numerical results with those of Refs. [39, 40]. However the perturbative input of Refs. [12, 13, 39, 40] and ours is identical.

new analysis has to be considered as accidental. As the outcome of our analysis we quantify the current $\mathcal{O}(\alpha_s^3)$ perturbative error as around 20 MeV, which is an order of magnitude larger than that of Refs. [12, 13, 39, 40].

2. Using a clustering method [46–48] to combine correlated data from many different experimental measurements we show that the e^+e^- total hadronic cross section relevant for the charmonium sum rules can be determined with a complete coverage of center of mass energies above the J/ψ and ψ' resonances up to 10.538 GeV. Conservatively estimated modeling uncertainties coming from the energy range above 10.538 GeV then only lead to an insignificant contribution to the total uncertainty of the experimental moments. We also take the opportunity to include recent updates concerning the data on ψ' charmonium resonance.

This paper is organized as follows: In Sec. 2 we introduce the theoretical framework and review the current status of perturbative computations. We also show various equivalent ways of arranging the perturbative series in α_s for the charm mass. Finally we discuss how to properly estimate theoretical uncertainties due to the truncation of the perturbative series. In Sec. 3 we present all the experimental information that goes into our analysis. We discuss a clustering fit procedure that allows to combine data from different experiments accounting for their correlation and show the results. In Sec. 4 we carry out the numerical charm mass analysis concentrating on the first moment M_1 using arbitrary values of α_s , and we present our final charm mass result. In Sec. 5 we discuss the charm mass results obtained from higher moments $M_{2,3,4}$ and find agreement with the outcome of the first moment analysis. In Appendix A we present more details on the outcome of our clustering fit procedure for the charm R -ratio, and in Appendix B we prove the equivalence of different versions of χ^2 functions when auxiliary fit parameters are employed. Appendix C shows the dependence of the higher moment charm mass results on the strong coupling.

2 Theoretical Input

2.1 Perturbative Contribution

The moments of the vector current correlator are defined in Eq. (1.1). Their perturbative contribution in the framework of the OPE has a non-linear dependence on the charm quark mass. Thus in principle no conceptual preference can be imposed on any of the possible perturbative series that arises when solving for the charm mass. As a consequence, different versions of the expansion should be considered to obtain reliable estimates of the perturbative uncertainty. As indicated in Sec. 1 we use in the following μ_α as the renormalization scale in α_s and μ_m as the renormalization scale in the $\overline{\text{MS}}$ charm quark mass \overline{m}_c .

(a) Standard fixed-order expansion

Writing the perturbative vacuum polarization function as

$$\Pi^{\text{pert}}(q^2, \alpha_s(\mu_\alpha), \overline{m}_c(\mu_m), \mu_\alpha, \mu_m) = \frac{1}{12\pi^2 Q_c^2} \sum_{n=0}^{\infty} q^{2n} M_n^{\text{pert}}, \quad (2.1)$$

	$C_{n,i}^{0,0}$	$C_{n,i}^{1,0}$	$C_{n,i}^{2,0}$	$C_{n,i}^{3,0}$	$C_{n,i}^{0,1}$	$C_{n,i}^{1,1}$	$C_{n,i}^{2,1}$	$C_{n,i}^{0,2}$	$C_{n,i}^{1,2}$
$n = 1$									
$i = 0$	1.06667	0	0	0	0	0	0	0	0
$i = 1$	2.55473	2.13333	0	0	0	0	0	0	0
$i = 2$	2.49671	8.63539	4.35556	0	-5.32236	-4.44444	0	0	0
$i = 3$	-5.64043	22.6663	32.696	8.95309	-18.5994	-42.8252	-18.1481	11.0882	9.25926
$n = 2$									
$i = 0$	0.457143	0	0	0	0	0	0	0	0
$i = 1$	1.10956	1.82857	0	0	0	0	0	0	0
$i = 2$	2.77702	7.46046	5.5619	0	-2.31158	-3.80952	0	0	0
$i = 3$	-3.49373	21.8523	38.6277	15.1407	-15.1307	-36.9519	-23.1746	4.81579	7.93651
$n = 3$									
$i = 0$	0.270899	0	0	0	0	0	0	0	0
$i = 1$	0.519396	1.6254	0	0	0	0	0	0	0
$i = 2$	1.63882	5.8028	6.56931	0	-1.08207	-3.38624	0	0	0
$i = 3$	-2.83951	16.0684	40.3042	22.2627	-8.4948	-29.3931	-27.3721	2.25432	7.05467
$n = 4$									
$i = 0$	0.184704	0	0	0	0	0	0	0	0
$i = 1$	0.203121	1.47763	0	0	0	0	0	0	0
$i = 2$	0.795555	4.06717	7.44974	0	-0.42317	-3.0784	0	0	0
$i = 3$	-3.349	8.91524	38.2669	30.2128	-3.96649	-21.6873	-31.0406	0.881603	6.41334

Table 1. Numerical values of the coefficients for Eq. (2.2). (Standard fixed-order expansion).

we have for the perturbative moments M_n^{pert}

$$M_n^{\text{pert}} = \frac{1}{(4\bar{m}_c^2(\mu_m))^n} \sum_{i,a,b} \left(\frac{\alpha_s(\mu_\alpha)}{\pi} \right)^i C_{n,i}^{a,b} \ln^a \left(\frac{\bar{m}_c^2(\mu_m)}{\mu_m^2} \right) \ln^b \left(\frac{\bar{m}_c^2(\mu_m)}{\mu_\alpha^2} \right). \quad (2.2)$$

This is the standard fixed-order expression for the perturbative moments. At $\mathcal{O}(\alpha_s^3)$ the coefficients $C_{n,3}^{0,0}$ were recently determined for $n = 1$ [12, 13], $n = 2$ [14], $n = 3$ [15] and higher [16–18]. We refer to Ref. [9, 11] for the coefficients at $\mathcal{O}(\alpha_s^2)$. For convenience we have summarized the numerical expressions for the $C_{n,i}^{a,b}$ coefficients of the first four moments in Tab. 1.

The standard fixed-order expansion in Eq. (2.2) is the common way to represent the perturbative moments. However, written in this form the non-linear dependence on \bar{m}_c does for some values of the experimental moments and the renormalization scales not yield numerical solutions⁵ for \bar{m}_c .

(b) Linearized expansion

Concerning the charm mass dependence, a more linear way to organize the perturbative expansion is to take the $2n$ -th root of Eq. (2.2):⁶

$$\left(M_n^{\text{th,pert}} \right)^{1/2n} = \frac{1}{2\bar{m}_c(\mu_m)} \sum_{i,a,b} \left(\frac{\alpha_s(\mu_\alpha)}{\pi} \right)^i \tilde{C}_{n,i}^{a,b} \ln^a \left(\frac{\bar{m}_c^2(\mu_m)}{\mu_m^2} \right) \ln^b \left(\frac{\bar{m}_c^2(\mu_m)}{\mu_\alpha^2} \right), \quad (2.3)$$

⁵This tends to happen frequently at any order in α_s for $n > 1$ and for $\mu_m \sim 3$ GeV.

⁶A similar expansion was employed in Ref. [42].

	$\tilde{C}_{n,i}^{0,0}$	$\tilde{C}_{n,i}^{1,0}$	$\tilde{C}_{n,i}^{2,0}$	$\tilde{C}_{n,i}^{3,0}$	$\tilde{C}_{n,i}^{0,1}$	$\tilde{C}_{n,i}^{1,1}$	$\tilde{C}_{n,i}^{2,1}$	$\tilde{C}_{n,i}^{0,2}$	$\tilde{C}_{n,i}^{1,2}$
$n = 1$									
$i = 0$	1.0328	0	0	0	0	0	0	0	0
$i = 1$	1.2368	1.0328	0	0	0	0	0	0	0
$i = 2$	0.46816	2.94379	1.59223	0	-2.57668	-2.15166	0	0	0
$i = 3$	-3.2913	6.97983	10.9784	2.74217	-5.91875	-15.5793	-6.63428	5.36808	4.48262
$n = 2$									
$i = 0$	0.822267	0	0	0	0	0	0	0	0
$i = 1$	0.498944	0.822267	0	0	0	0	0	0	0
$i = 2$	0.79463	1.85797	1.26766	0	-1.03947	-1.71306	0	0	0
$i = 3$	-3.20128	3.15216	7.99164	2.1832	-4.91174	-10.3796	-5.28192	2.16555	3.56887
$n = 3$									
$i = 0$	0.804393	0	0	0	0	0	0	0	0
$i = 1$	0.257044	0.804393	0	0	0	0	0	0	0
$i = 2$	0.605688	1.58653	1.24011	0	-0.535508	-1.67582	0	0	0
$i = 3$	-2.46047	1.56737	7.46171	2.13574	-3.34838	-9.19128	-5.1671	1.11564	3.49129
$n = 4$									
$i = 0$	0.809673	0	0	0	0	0	0	0	0
$i = 1$	0.111301	0.809673	0	0	0	0	0	0	0
$i = 2$	0.382377	1.44951	1.24825	0	-0.231877	-1.68682	0	0	0
$i = 3$	-2.21776	0.492406	7.2834	2.14976	-1.95033	-8.63733	-5.20102	0.483077	3.51421

Table 2. Numerical values of the coefficients for Eq. (2.3). (Linearized expansion).

or equivalently

$$\bar{m}_c(\mu_m) = \frac{1}{2(M_n^{\text{th,pert}})^{1/2n}} \sum_{i,a,b} \left(\frac{\alpha_s(\mu_\alpha)}{\pi} \right)^i \tilde{C}_{n,i}^{a,b} \ln^a \left(\frac{\bar{m}_c^2(\mu_m)}{\mu_m^2} \right) \ln^b \left(\frac{\bar{m}_c^2(\mu_m)}{\mu_\alpha^2} \right). \quad (2.4)$$

The coefficients $\tilde{C}_{n,i}^{a,b}$ using again μ_α for the renormalization scale in α_s and μ_m for the renormalization scale in the $\overline{\text{MS}}$ charm mass are given in Tab. 2. Although relation (2.4) involves a non-linear dependence on \bar{m}_c , we find that it always has a numerical solution.

(c) Iterative linearized expansion

For the standard and the linearized expansions in Eqs. (2.2) and (2.3) one searches for numerical solutions of the charm mass $\bar{m}_c(\mu_m)$ keeping the exact mass dependence on the respective RHS at each order in α_s . An alternative way that is consistent within perturbation theory is to solve for $\bar{m}_c(\mu_m)$ iteratively order-by-order supplementing appropriate lower order values for $\bar{m}_c(\mu_m)$ in higher order perturbative coefficients. To be more explicit, we describe the method in the following. As the basis for the iterative expansion carried out in our analysis we use the linearized expansion of Eq. (2.4).

In the first step we determine $\bar{m}_c(\mu_m)$ employing the tree-level relation

$$\bar{m}_c^{(0)} = \frac{1}{2(M_n^{\text{th,pert}})^{1/2n}} \tilde{C}_{n,0}^{0,0}, \quad (2.5)$$

giving the tree-level charm mass $\bar{m}_c^{(0)}$. In the next step one employs the relation

$$\bar{m}_c^{(1)}(\mu_m) = \frac{1}{2(M_n^{\text{th,pert}})^{1/2n}} \left\{ \tilde{C}_{n,0}^{0,0} + \frac{\alpha_s(\mu_\alpha)}{\pi} \left[\tilde{C}_{n,1}^{0,0} + \tilde{C}_{n,1}^{1,0} \ln \left(\frac{\bar{m}_c^{(0)2}}{\mu_m^2} \right) \right] \right\}, \quad (2.6)$$

to determine the $\mathcal{O}(\alpha_s)$ charm mass $\bar{m}_c^{(1)}(\mu_m)$. In the $\mathcal{O}(\alpha_s)$ terms on the RHS of Eq. (2.6) the tree-level charm mass $\bar{m}_c^{(0)}$ is used, which is consistent to $\mathcal{O}(\alpha_s)$. At $\mathcal{O}(\alpha_s^2)$ for the determination of $\bar{m}_c^{(2)}(\mu_m)$ one uses $\bar{m}_c^{(0)}$ for the $\mathcal{O}(\alpha_s^2)$ coefficient and $\bar{m}_c^{(1)}(\mu_m)$ for the $\mathcal{O}(\alpha_s)$ correction, which in the strict α_s expansion yields

$$\begin{aligned} \bar{m}_c^{(2)}(\mu_m) = & \frac{1}{2(M_n^{\text{th,pert}})^{1/2n}} \left\{ \tilde{C}_{n,0}^{0,0} + \frac{\alpha_s(\mu_\alpha)}{\pi} \left[\tilde{C}_{n,1}^{0,0} + \tilde{C}_{n,1}^{1,0} \ln \left(\frac{\bar{m}_c^{(0)2}}{\mu_m^2} \right) \right] + \right. \\ & \left(\frac{\alpha_s(\mu_\alpha)}{\pi} \right)^2 \left[2 \frac{\tilde{C}_{n,1}^{1,0} \tilde{C}_{n,1}^{0,0}}{\tilde{C}_{n,0}^{0,0}} + 2 \frac{(\tilde{C}_{n,1}^{1,0})^2}{\tilde{C}_{n,0}^{0,0}} \ln \left(\frac{\bar{m}_c^{(0)2}}{\mu_m^2} \right) + \right. \\ & \left. \left. \sum_{a,b} \tilde{C}_{n,2}^{a,b} \ln^a \left(\frac{\bar{m}_c^{(0)2}}{\mu_m^2} \right) \ln^b \left(\frac{\bar{m}_c^{(0)2}}{\mu_\alpha^2} \right) \right] \right\}. \end{aligned} \quad (2.7)$$

Here the second line contains the derivative of the $\mathcal{O}(\alpha_s)$ terms with respect to the charm mass. The determination of the $\mathcal{O}(\alpha_s^3)$ charm mass $\bar{m}_c^{(3)}(\mu_m)$ is then carried out in an analogous way involving the second (first) derivative with respect to the mass in the $\mathcal{O}(\alpha_s)$ ($\mathcal{O}(\alpha_s^2)$) correction and using again $\bar{m}_c^{(0)}$ for the $\mathcal{O}(\alpha_s^3)$ coefficient.

In general we can write the iterative expansion as follows:

$$\bar{m}_c(\mu_m) = \bar{m}_c^{(0)} \sum_{i,a,b} \left(\frac{\alpha_s(\mu_\alpha)}{\pi} \right)^i \hat{C}_{n,i}^{a,b} \ln^a \left(\frac{\bar{m}_c^{(0)2}}{\mu_m^2} \right) \ln^b \left(\frac{\bar{m}_c^{(0)2}}{\mu_\alpha^2} \right), \quad (2.8)$$

where the numerical value of the coefficients $\hat{C}_{n,i}^{a,b}$ are collected in Tab. 3.

The iterative way to treat the perturbative series for the charm mass has the advantage that solving for the charm mass involves equations that are strictly linear in the charm mass at any order of the α_s expansion and thus by construction always have solutions. In this way any possible influence on the analysis arising from a non-linear dependence is eliminated.

(d) Contour improved expansion

For the expansion methods (a)-(c) the moments and the charm quark mass are computed for a fixed choice of the renormalization scale μ_α in the strong coupling α_s . In analogy to the contour improved methods used for τ -decays (see e.g. Refs. [49–54]) one can employ a path-dependent μ_α in the contour integration that defines the perturbative moments [38], see Fig. 1,

$$M_n^{\text{c,pert}} = \frac{6\pi Q_c^2}{i} \int_c \frac{ds}{s^{n+1}} \Pi(q^2, \alpha_s(\mu_\alpha^c(s, \bar{m}_c^2)), \bar{m}_c(\mu_m), \mu_\alpha^c(s, \bar{m}_c^2), \mu_m). \quad (2.9)$$

Due to the independence of the moments on μ_α and since no large logarithms are being

	$\hat{C}_{n,i}^{0,0}$	$\hat{C}_{n,i}^{1,0}$	$\hat{C}_{n,i}^{2,0}$	$\hat{C}_{n,i}^{3,0}$	$\hat{C}_{n,i}^{0,1}$	$\hat{C}_{n,i}^{1,1}$	$\hat{C}_{n,i}^{2,1}$	$\hat{C}_{n,i}^{0,2}$	$\hat{C}_{n,i}^{1,2}$
$n = 1$									
$i = 0$	1	0	0	0	0	0	0	0	0
$i = 1$	1.19753	1	0	0	0	0	0	0	0
$i = 2$	2.84836	4.85031	1.54167	0	-2.49486	-2.08333	0	0	0
$i = 3$	1.92718	17.1697	14.7131	2.65509	-15.7102	-23.418	-6.42361	5.19762	4.34028
$n = 2$									
$i = 0$	1	0	0	0	0	0	0	0	0
$i = 1$	0.60679	1	0	0	0	0	0	0	0
$i = 2$	2.17997	4.25957	1.54167	0	-1.26415	-2.08333	0	0	0
$i = 3$	1.30653	14.3435	13.8024	2.65509	-11.03	-20.9565	-6.42361	2.63364	4.34028
$n = 3$									
$i = 0$	1	0	0	0	0	0	0	0	0
$i = 1$	0.31955	1	0	0	0	0	0	0	0
$i = 2$	1.39208	3.97233	1.54167	0	-0.66573	-2.08333	0	0	0
$i = 3$	0.458292	12.5064	13.3595	2.65509	-6.82554	-19.7597	-6.42361	1.38694	4.34028
$n = 4$									
$i = 0$	1	0	0	0	0	0	0	0	0
$i = 1$	0.137464	1	0	0	0	0	0	0	0
$i = 2$	0.747189	3.79024	1.54167	0	-0.286383	-2.08333	0	0	0
$i = 3$	-0.850143	11.1964	13.0788	2.65509	-3.55432	-19.001	-6.42361	0.596632	4.34028

Table 3. Numerical values of the coefficients for Eq. (2.8). (Iterative linearized expansion).

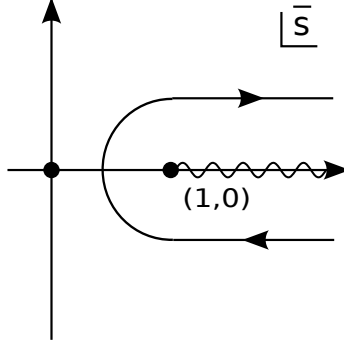


Figure 1. Path of integration in the complex \bar{s} -plane for the computation of the moments.

generated anywhere for a path with distance of order \bar{m}_c from the cut on the real axis, this method is a viable alternative to carry out the perturbative expansion. The different orders in the expansion of the contour improved moments $M_n^{c,\text{pert}}$ are generated from the fixed-order α_s expansion of the vacuum polarization function Π in Eq. (2.9).

A useful path-dependent choice for μ_α^c is given by [38]

$$(\mu_\alpha^c)^2(s, \bar{m}_c^2) = \mu_\alpha^2 \left(1 - \frac{s}{4\bar{m}_c^2(\mu_m)} \right), \quad (2.10)$$

which implements a modified weighting of threshold versus high energy contributions. It is straightforward to prove that the resulting moments $M_n^{c,\text{pert}}$ can be obtained from the

	$C_{0,i}^{0,0}$	$C_{0,i}^{1,0}$	$C_{0,i}^{0,1}$	$C_{0,i}^{0,2}$
$i = 0$	0	0	0	0
$i = 1$	1.44444	0	0	0
$i = 2$	2.83912	0	-3.00926	0
$i = 3$	-5.28158	6.01852	-16.4639	6.26929

Table 4. Numerical values of the coefficients for Eq. (2.12). ($\Pi(0)$ in the $\overline{\text{MS}}$ scheme.)

small- q^2 expansion of the perturbative vacuum polarization function using μ_α^c as the renormalization scale of α_s ,

$$\Pi^{\overline{\text{MS}}}(q^2, \alpha_s(\mu_\alpha^c(q^2, \overline{m}_c^2)), \overline{m}_c(\mu_m), \mu_\alpha^c(q^2, \overline{m}_c^2), \mu_m) = \sum_{n=0}^{\infty} q^{2n} M_n^{\text{c,pert}}. \quad (2.11)$$

From Eq. (2.11) we can see that the $M_n^{\text{c,pert}}$ can be derived from the expressions for the fixed-order moments M_m^{pert} with $m \leq n$ given in Eq. (2.2).⁷ They also depend on the QCD β -function and its derivatives, which arise in the small- q^2 expansion of $\alpha_s(\mu_\alpha^c(q^2, \overline{m}_c^2))$. Note that the β -function that has to be employed must be exactly the same that is used for the contour integration in Eq. (2.9). Expanding the dependence of the β -function on α_s strictly in fixed-order one recovers the fixed-order moments M_n^{pert} . So the dependence of the contour improved moments $M_n^{\text{c,pert}}$ on the fixed-order moments M_m^{pert} with $m < n$ is only residual due to the truncation of the α_s series and vanishes in the large order limit. The contour improved expansion thus represents yet another alternative parametrization of higher order perturbative corrections. Due to their residual dependence on lower moments the contour improved moments have a sensitivity to the UV-subtraction scheme for the vacuum polarization function, i.e. on $\Pi(0) = M_0^{\text{pert}}$. Using the “on-shell” scheme with $\Pi(0) = 0$ one finds that $M_1^{\text{c,pert}} = M_1^{\text{pert}}$. For our analysis we employ the $\overline{\text{MS}}$ scheme for $\Pi(0)$ defined for $\mu = \overline{m}_c(\overline{m}_c)$. Expressed in terms of $\alpha_s(\mu_\alpha)$ and $\overline{m}_c(\mu_m)$ it has the form [12]

$$\Pi^{\overline{\text{MS}}}(0) = \sum_{i,a,b} \left(\frac{\alpha_s(\mu_\alpha)}{\pi} \right)^i C_{0,i}^{a,b} \ln^a \left(\frac{\overline{m}_c^2(\mu_m)}{\mu_m^2} \right) \ln^b \left(\frac{\overline{m}_c^2(\mu_m)}{\mu_\alpha^2} \right). \quad (2.12)$$

The numerical values for the coefficients $C_{0,i}^{a,b}$ can be found in Tab. 4. Using contour improved moments to determine \overline{m}_c also involves non-linear relations, which implies that in some cases there is no solution. Again this can happen for $n \geq 1$ and for $\mu_m \sim 3$ GeV at any order.

⁷ This works in general as long as the path dependent $\mu_\alpha^c(q^2, \overline{m}_c^2)$ does not produce a spurious cut in α_s starting at $q^2 = 0$ and running towards $-\infty$. This condition is implemented into Eq. (2.10) by $(\mu_\alpha^c)^2$ being negative along the physical cut of the vacuum polarization function above the charm pair threshold.

	$n = 1$	$n = 2$	$n = 3$	$n = 4$
$a_n^{0,0}$	-16.042	-26.7367	-38.8898	-52.3516
$a_n^{1,0}$	-143.364	-272.186	-439.820	-646.690

Table 5. Numerical values for the coefficients of Eq. (2.14). (Gluon condensate contribution).

2.2 Gluon Condensate Contribution

The dominant subleading contribution in the OPE for the theory moments M_n^{th} is arising from the gluon condensate giving [2, 55]

$$M_n^{\text{th}} = M_n^{\text{pert}} + \Delta M_n^{(G^2)} + \dots, \quad (2.13)$$

where the ellipses represent higher order power-suppressed condensate contributions of the OPE. The $\mathcal{O}(\alpha_s)$ corrections to the Wilson coefficient of the gluon condensate corrections have been determined in Ref. [19]. In Ref. [56] it is suggested that the Wilson coefficient of the gluon condensate should be expressed in terms of the pole rather than the $\overline{\text{MS}}$ mass based on the observation that the pole mass leads to a condensate correction that is numerically quite stable for higher moments. We confirm this behavior, and mention that it results from the strong inverse power-dependence on the charm mass that generates a large n -dependence in the $\mathcal{O}(\alpha_s)$ corrections. Since we parameterize all mass dependence in terms of the $\overline{\text{MS}}$ charm mass, we adopt an analytic expression for the gluon condensate correction, where the corrections associated to the pole mass are grouped together with the $\overline{\text{MS}}$ charm mass parameter. The resulting expression reads

$$\begin{aligned} \Delta M_n^{(G^2)} &= \frac{1}{(4M_c^2)^{n+2}} \left\langle \frac{\alpha_s}{\pi} G^2 \right\rangle_{\text{RGI}} \left[a_n^{0,0} + \frac{\alpha_s(\mu_\alpha)}{\pi} a_n^{1,0} \right], \\ M_c &= \overline{m}_c(\mu_m) \left\{ 1 + \frac{\alpha_s(\mu_\alpha)}{\pi} \left[\frac{4}{3} - \ln \left(\frac{\overline{m}_c^2(\mu_m)}{\mu_\mu^2} \right) \right] \right\}, \end{aligned} \quad (2.14)$$

using the renormalization group invariant (RGI) scheme for the gluon condensate [57]. Numerical values for the coefficients $a_n^{i,j}$ are given in Tab. 5 for $n = 1, 2, 3, 4$. For the RGI gluon condensate we adopt [58]

$$\left\langle \frac{\alpha_s}{\pi} G^2 \right\rangle_{\text{RGI}} = 0.006 \pm 0.012 \text{ GeV}^4. \quad (2.15)$$

The overall contribution of the gluon condensate correction in Eq. (2.14) in the charm quark mass analysis is quite small. Its contribution to the moments amounts to around 0.4%, 2%, 5%, and 9% for the first four moments, respectively. For $n = 1$ it leads to a correction in the $\overline{\text{MS}}$ charm quark mass at the level of 2 MeV and is an order of magnitude smaller than our perturbative uncertainty. We therefore ignore the condensate correction for the discussion of the perturbative uncertainties in Sec. 2.4. Its contribution is, however, included for completeness in the final charm mass results presented in Secs. 4 and 5.

2.3 Running Coupling and Mass

The analysis of the charmonium sum rules naturally involves renormalization scales around the charm mass, $\mu \sim \bar{m}_c \sim 1.3$ GeV, which are close to the limits of a perturbative treatment. In fact, parametrically, the typical scale relevant for the perturbative computation of the n -th moment M_n^{th} is of order $\mu \sim \bar{m}_c/n$ (see e.g. Ref. [59]) because the energy range of the smearing associated to the weight function $1/s^{n+1}$ in Eq. (1.2) decreases with n . We will therefore use $n = 1$ for our final numerical analysis. Moreover, it is common practice to quote the $\overline{\text{MS}}$ charm mass $\bar{m}_c(\bar{m}_c)$, i.e. for the scale choice $\mu_m = \bar{m}_c$. It is therefore useful to have a look at the quality of the perturbative behavior of the renormalization group evolution of the strong $\overline{\text{MS}}$ coupling α_s and the $\overline{\text{MS}}$ charm quark mass.

In Fig. 2(a)⁸ we have displayed $\alpha_s^{\text{N}^3\text{LL}}(\mu)/\alpha_s^{\text{N}^k\text{LL}}(\mu)$ using for $\alpha_s^{\text{N}^k\text{LL}}$ the $(k+1)$ -loop QCD β -function and the respective exact numerical solution for $\alpha_s(3 \text{ GeV}) = 0.2535$ as the common reference point. We see that the convergence of the lower order results towards the 4-loop evolution is very good even down to scales of around 1 GeV. The curves indicate that the remaining relative perturbative uncertainty in the 4-loop evolution might be substantially smaller than 1% for scales down to $\bar{m}_c \sim 1.3$ GeV. It is also instructive to examine the evolution using a fixed-order expansion. In Fig. 2(b) we display $\alpha_s^{\text{N}^3\text{LL}}(\mu)/\alpha_s^{(m)}(\mu)$ where $\alpha_s^{(m)}(\mu)$ is the $\mathcal{O}(\alpha_s^{m+1})$ fixed-order expression for $\alpha_s(\mu)$ using the reference value $\alpha_s(3 \text{ GeV}) = 0.2535$ as the expansion parameter. The convergence of the fixed-order expansion for $\alpha_s(\mu)$ towards the exact N³LL numerical solution $\alpha_s^{\text{N}^3\text{LL}}(\mu)$ is somewhat worse compared to the renormalization group resummed results since the deviation of the ratio from one is in general larger. However, convergence is clearly visible. In particular there are not any signs of instabilities. It therefore seems to be safe to use renormalization scales down to the charm mass and associated renormalization scale variations as an instrument to estimate the perturbative uncertainties.

In Figs. 3(a) and 3(b) an analogous analysis has been carried out for the $\overline{\text{MS}}$ charm quark mass. In Fig. 3(a) $\bar{m}_c^{\text{N}^3\text{LL}}(\mu)/\bar{m}_c^{\text{N}^k\text{LL}}(\mu)$ is plotted for $k = 0, 1, 2, 3$ using the exact numerical solutions of the $(k+1)$ -loop renormalization group equations and $\bar{m}_c(\mu = 3 \text{ GeV})$ as the respective reference value.⁹ Compared to the Fig. 2 we observe a very similar convergence. In Fig. 3(b), finally, we show $\bar{m}_c^{\text{N}^3\text{LL}}(\mu)/\bar{m}_c^{(m)}(\mu)$, where $\bar{m}_c^{(m)}(\mu)$ is the $\mathcal{O}(\alpha_s^m)$ fixed-order expression for $\bar{m}_c(\mu)$ using $\alpha_s(3 \text{ GeV}) = 0.2535$ as the expansion parameter. Again, the convergence towards the exact N³LL evolved result is very similar to the corresponding results for the strong coupling, and we find again no evidence for perturbative instabilities. Of course the corrections are somewhat larger when the fixed-order expansion is employed. We therefore conclude that perturbative evolution and renormalization scale variations for the $\overline{\text{MS}}$ charm quark mass can be safely used down to scales above $\bar{m}_c \sim 1.3$ GeV. One should of course mention that the lines in Fig. 3(b) also give an indication about the expected size of scale variations depending on the range of the variations.

⁸ In this examination and throughout our other analyses we use the $\overline{\text{MS}}$ renormalization group equations with $n_f = 4$ active running flavors.

⁹ The numerical value of $\bar{m}_c(\mu = 3 \text{ GeV})$ is actually irrelevant, since the running involves \bar{m}_c only in a linear way and exactly cancels in the ratio.

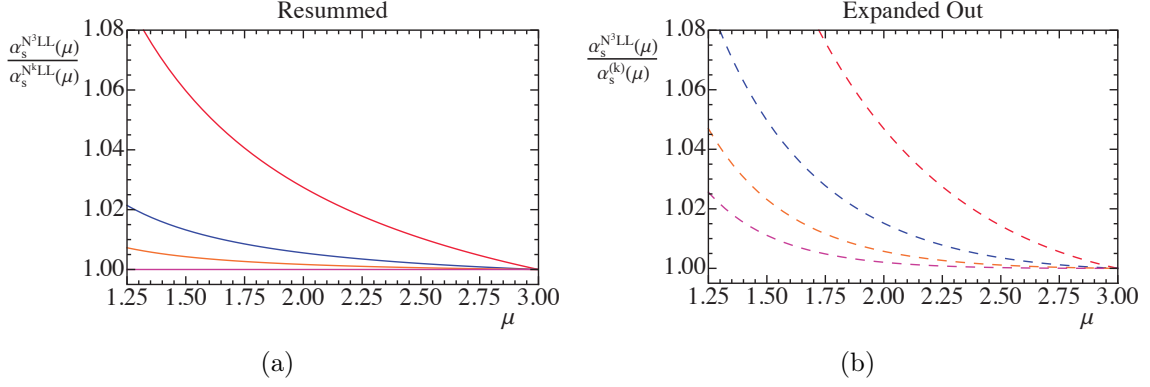


Figure 2. Results for $\alpha_s^{N^3LL}(\mu)/\alpha_s^{N^kLL}(\mu)$ (a) and $\alpha_s^{N^3LL}(\mu)/\alpha_s^{(k)}(\mu)$ (b), where $\alpha_s^{N^kLL}$ stands for the $(k+1)$ -loop running coupling constant and $\alpha_s^{(k)}$ is the corresponding $\mathcal{O}(\alpha_s^{(k+1)})$ fixed-order expression for α_s . All orders are run from the common point $\alpha_s(3 \text{ GeV}) = 0.2535$.

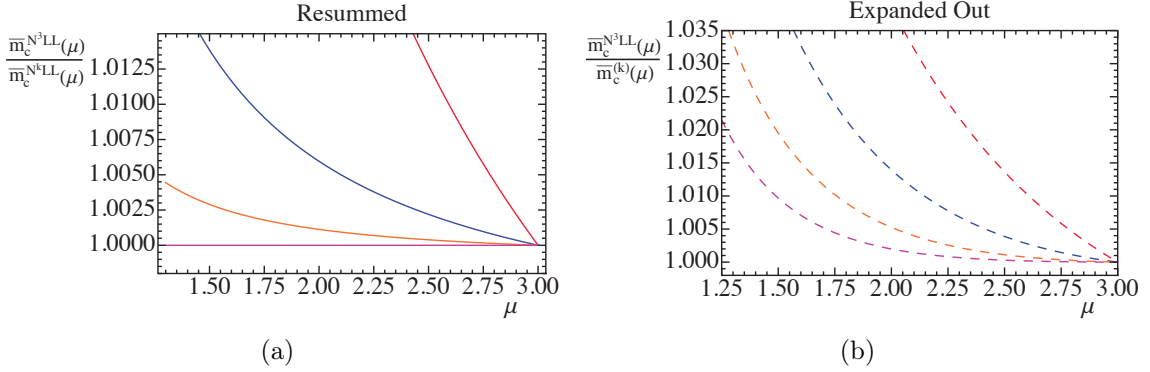


Figure 3. Results for $\overline{m}_c^{N^3LL}(\mu)/\overline{m}_c^{N^kLL}(\mu)$ (a) and $\overline{m}_c^{N^3LL}(\mu)/\overline{m}_c^{(k)}(\mu)$ (b), where $\overline{m}_c^{N^kLL}$ stands for the $(k+1)$ -loop running $\overline{\text{MS}}$ charm mass and $\overline{m}_c^{(k)}$ is the $\mathcal{O}(\alpha_s^{(k+1)})$ fixed-order expression.

Scales above 2 GeV can lead to sub-MeV variations, while scales down to the charm mass will result in percent precision (i.e. $\mathcal{O}(10 \text{ MeV})$).

2.4 Perturbative Uncertainties in the $\overline{\text{MS}}$ Charm Mass

In this section we discuss in detail the perturbative series for the determination of the $\overline{\text{MS}}$ charm mass \overline{m}_c and how to set up an adequate scale variation to estimate the perturbative uncertainty. In the previous subsections we have discussed four different ways to carry out the perturbative expansion and we presented the corresponding order-by-order analytic expressions. As described there, we can determine at each order of the perturbative expansion for the moments M_n^{th} a value for $\overline{m}_c(\mu_m)$ which also has a residual dependence on μ_α , the renormalization scale used for α_s . To compare the different mass determinations we then evolve $\overline{m}_c(\mu_m)$ to obtain $\overline{m}_c(\overline{m}_c)$ using the 4-loop renormalization group equations for the mass and the strong coupling [60–64].¹⁰ The obtained value of $\overline{m}_c(\overline{m}_c)$ thus has a

¹⁰ For the discussions in this section we use $\alpha_s^{(n_f=5)}(m_Z) = 0.118$ ($\alpha_s^{(n_f=4)}(4.2 \text{ GeV}) = 0.2245$) as an input using five-to-four flavor matching at 4.2 GeV. For the first moment employed for the charm mass fits

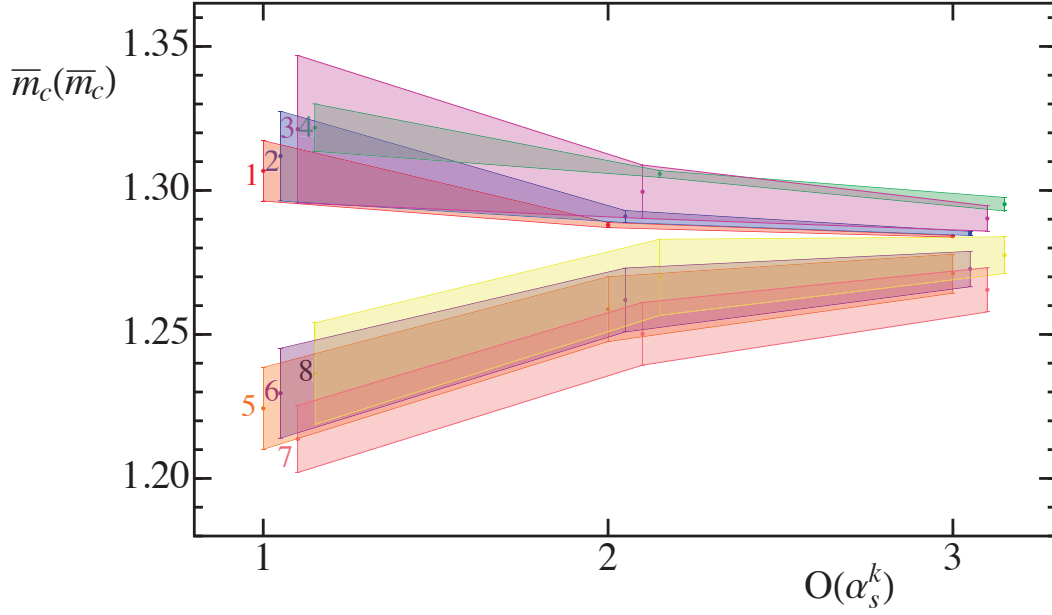


Figure 4. Results for $\overline{m}_c(\overline{m}_c)$ at various orders, for methods a (graphs 1 and 5), b (2,6), c (3,7), and d (4,8), setting $\mu_\alpha = \mu_m$ (graphs 1-4) and setting $\mu_m = \overline{m}_c(\overline{m}_c)$ (5-8). The shaded regions arise from the variation $2 \text{ GeV} \leq \mu_\alpha \leq 4 \text{ GeV}$.

residual dependence on the scales μ_m and μ_α , on the order of perturbation theory and on the expansion method.¹¹ For the results we can therefore use the notation

$$\overline{m}_c(\overline{m}_c)[\mu_m, \mu_\alpha]^{i,n}, \quad (2.16)$$

where $n = 0, 1, 2, 3$ indicates perturbation theory at $\mathcal{O}(\alpha_s^n)$ and

$$i = \begin{cases} a & \text{(fixed-order expansion),} \\ b & \text{(linearized expansion),} \\ c & \text{(iterative expansion),} \\ d & \text{(contour improved expansion).} \end{cases} \quad (2.17)$$

To initiate the discussion, we show in Fig. 4 results for $\overline{m}_c(\overline{m}_c)$ at $\mathcal{O}(\alpha_s^n)$ for expansions a–d using $\mu_m = \mu_\alpha$ (upper four graphs) and using $\mu_m = \overline{m}_c(\overline{m}_c)$ (lower four graphs). For each method and order we have displayed the range of $\overline{m}_c(\overline{m}_c)$ values for a variation of $2 \text{ GeV} \leq \mu_\alpha \leq 4 \text{ GeV}$, which corresponds to the scale variation employed in Refs. [12, 13, 39, 40]. Their analysis used the fixed-order expansion with the setting $\mu_m = \mu_\alpha$ and is represented by graph 1. We make several observations:

- (i) Choosing μ_m and μ_α both larger than 2 GeV makes the $\overline{m}_c(\overline{m}_c)$ value decrease with the order of perturbation theory.

we use $M_1 = 0.2138 \text{ GeV}^{-1}$.

¹¹Of course the extracted mass depends on the moment considered as well. Since in our analysis we focus on the first moment only, for simplicity we drop that label.

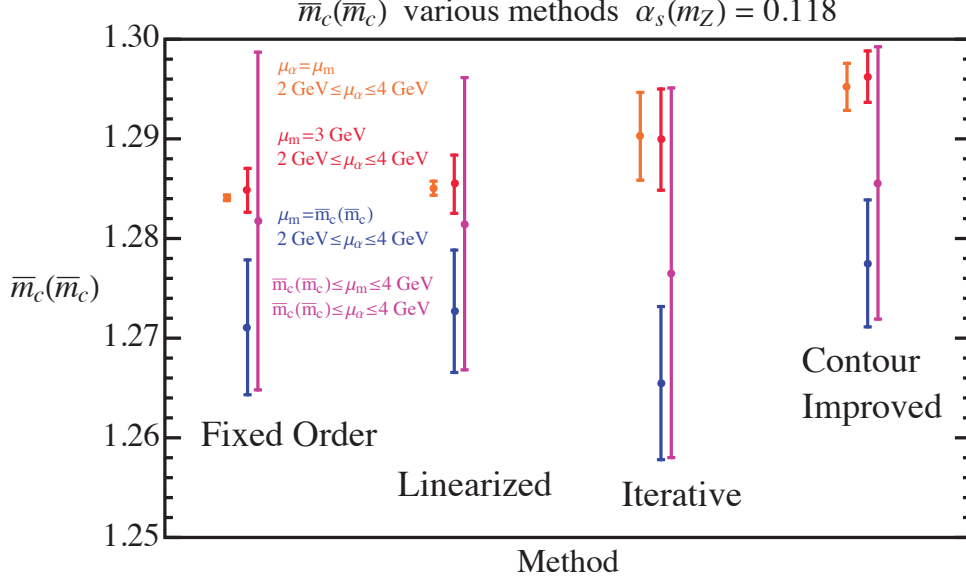


Figure 5. Estimates of the perturbative error at $\mathcal{O}(\alpha_s^3)$. We show the correlated $\mu_m = \mu_\alpha$ variation, (orange), setting $\mu_m = \bar{m}_c(\bar{m}_c)$ and setting $\mu_m = 3$ GeV, (blue and red, respectively), and the double scale variation (magenta).

- (ii) Choosing μ_m smaller than 1.5 GeV and μ_α larger than 2 GeV makes the $\bar{m}_c(\bar{m}_c)$ value increase with the order of perturbation theory.
- (iii) For most choices of the scale setting and the expansion method the spread of the $\bar{m}_c(\bar{m}_c)$ values from the variation of μ_α does not decrease in any substantial way with the order. However, viewing all methods and scale setting choices collectively a very good convergence is observed.

We have checked that these statements apply also in general beyond the specific cases displayed in Fig. 4.

Quite conspicuous results are obtained for the scale choice $\mu_m = \mu_\alpha$ for the fixed-order (graph 1) and linearized expansions (graph 2). Here, extremely small variations in $\bar{m}_c(\bar{m}_c)$ are obtained. They amount to 1.8 MeV (4 MeV) and 0.6 MeV (1.4 MeV) at order α_s^2 and α_s^3 , respectively, for the fixed-order expansions (linearized expansions). We note that our scale variation for the fixed-order expansion at $\mathcal{O}(\alpha_s^3)$ is consistent with the corresponding numbers quoted in Ref. [12, 13], where the $\mathcal{O}(\alpha_s^3)$ corrections to the first moment were computed,¹² but differs from the scale variations given in Refs. [39, 40] which also quoted numerical results from the fixed-order expansion. Interestingly the $\mathcal{O}(\alpha_s^2)$ and $\mathcal{O}(\alpha_s^3)$ variations we find do not overlap and the $\mathcal{O}(\alpha_s^3)$ ranges appear to be highly inconsistent with the $\mathcal{O}(\alpha_s^3)$ results from the iterative method (graph 3). A visual display of scale variations obtained from the four expansion methods at $\mathcal{O}(\alpha_s^3)$ with different types of variation methods is given in Fig. 5.

¹² We are grateful to Thomas Schutzmeier for confirming agreement of the results of our $\mathcal{O}(\alpha_s^3)$ fixed-order code with theirs of Ref. [13].

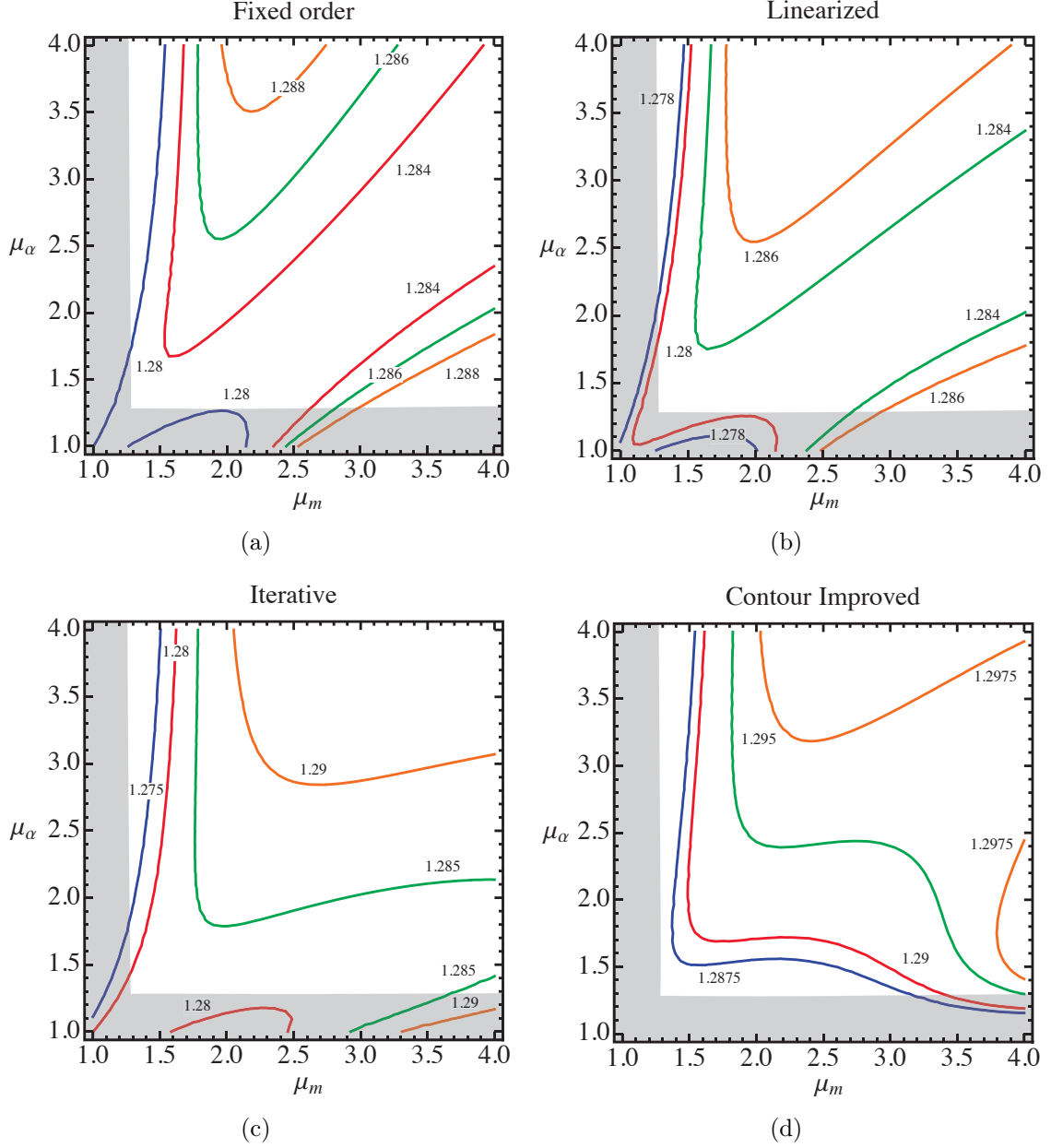


Figure 6. Contour plots for $\bar{m}_c(\bar{m}_c)$ as a function of μ_α and μ_m at $\mathcal{O}(\alpha_s^3)$, for methods (a)–(d). The shaded areas represent regions with $\mu_m, \mu_\alpha < \bar{m}_c(\bar{m}_c)$, and are excluded of our analysis.

An illustrative way to demonstrate how a small scale variation can arise is given in Fig. 6(a) - 6(d). For all four expansion methods contour curves of constant $\bar{m}_c(\bar{m}_c)$ are displayed as a function of (the residual dependence on) μ_m and μ_α . For the fixed-order (a) and the linearized expansions (b) we see that there are contour lines closely along the diagonal $\mu_m = \mu_\alpha$. For the fixed-order expansion (a) this feature is almost exact and thus explains the extremely small scale-dependence seen in graph 1 of Fig. 4. For the linearized expansion (b) this feature is somewhat less exact and reflected in the slightly larger scale

variation seen in graph 2 of Fig. 4. On the other hand, the contour lines of the iterative (c) and contour improved (d) expansions have a large angle with respect to the diagonal $\mu_m = \mu_\alpha$ leading to the much larger scale variations of 9 and 5 MeV, respectively, at $\mathcal{O}(\alpha_s^3)$ visible in graphs 3 and 4 of Fig. 4. The contour plots shown in Fig. 6 also show the variation along the line μ_m or $\mu_\alpha = \bar{m}_c(\bar{m}_c)$ (border of gray shaded areas). Here, the contour lines are relatively dense leading to scale variation of around 15 MeV at $\mathcal{O}(\alpha_s^3)$.

Overall, we draw the following conclusions:

- (1) The small scale variations observed for the fixed-order and linearized expansions for $\mu_m = \mu_\alpha$ result from strong cancellations of the individual μ_m and μ_α dependences that arise for this correlation.
- (2) Other correlations between μ_m and μ_α that do not generate large logarithms do not lead to such cancellations. One therefore has to consider the small scale variations observed for $\mu_m = \mu_\alpha$ in the fixed-order and linearized expansions as accidental.
- (3) For an adequate estimate of perturbative uncertainties specific correlations between μ_m and μ_α that are along contour lines of constant $\bar{m}_c(\bar{m}_c)$ have to be avoided. Moreover, adequate independent variations of μ_m and μ_α should not induce large logarithms.

As the outcome of this discussion we adopt for our charm mass analysis an independent and uncorrelated variation of μ_m and μ_α in the range

$$\bar{m}_c(\bar{m}_c) \leq \mu_m, \mu_\alpha \leq 4 \text{ GeV}, \quad (2.18)$$

in order to estimate perturbative uncertainties. The excluded region $\mu_m, \mu_\alpha < \bar{m}_c(\bar{m}_c)$ in the μ_m - μ_α plane in the contour plots of Fig. 6 is indicated by the gray shaded areas. This two-dimensional variation avoids accidental cancellations from correlated μ_m - μ_α variations, large logarithms involving ratios of the scales $\bar{m}_c(\mu_m)$, μ_m , μ_α and remains well in the validity ranges for the perturbative renormalization group evolution of the $\overline{\text{MS}}$ charm quark mass and α_s (see Sec. 2.3). The range of Eq. (2.18) is also consistent with a scale variation $\mu \sim 2\bar{m}_c \times (1/2, 1, 2)$ one might consider as the standard choice with respect to the to particle threshold located at $\sqrt{s} = 2\bar{m}_c$. As a comparison the range $\mu = (3 \pm 1) \text{ GeV}$ corresponds to $\mu = 2\bar{m}_c(0.8, 1.2, 1.6)$. We emphasize that the lower boundary $\bar{m}_c(\bar{m}_c) \sim 1.25 \text{ GeV}$ is also reasonable as it represents the common flavor matching scale where gauge coupling evolution remains smooth up to NLL order. We do not see any evidence for perturbation theory for the first moment M_1 being unstable at the charm mass scale, in contrast to claims made in Ref. [40].

In Fig. 7(a) we show the ranges of $\bar{m}_c(\bar{m}_c)$ at $\mathcal{O}(\alpha_s^{1,2,3})$ for the four expansion methods employing the scale variations of Eq. (2.18). We see that all four expansion methods now lead to equivalent results. The variations are also compatible with the overall variations shown in Fig. 4. At $\mathcal{O}(\alpha_s^3)$ we obtain a scale variation for $\bar{m}_c(\bar{m}_c)$ of around 20 MeV. This is an order of magnitude larger than the perturbative uncertainties quoted in Refs. [12, 13, 39, 40]. In Fig. 7(b) we have displayed the corresponding results for $\bar{m}_c(3 \text{ GeV})$. At $\mathcal{O}(\alpha_s^3)$ they also exhibit a scale variation of around 20 MeV.

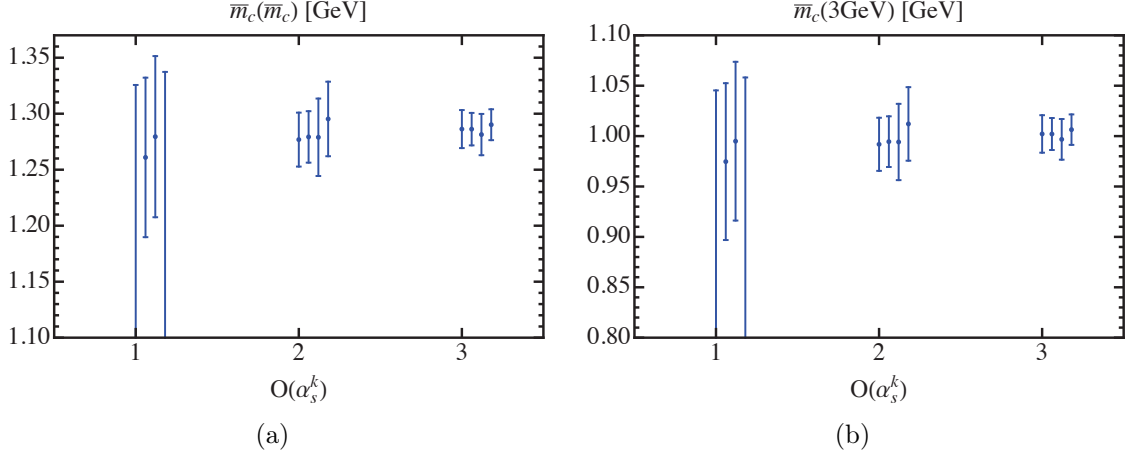


Figure 7. Results for $\bar{m}_c(\bar{m}_c)$ (a) and $\bar{m}_c(3\text{ GeV})$ (b), for methods a–d, at orders $\mathcal{O}(\alpha_s^{1,2,3})$. At $\mathcal{O}(\alpha_s^1)$ the error bars for fixed-order and contour improved methods extend down to 0.7 GeV for $\bar{m}_c(\bar{m}_c)$ and 0.4 GeV for $\bar{m}_c(3\text{ GeV})$.

	J/ψ	ψ'
M (GeV)	3.096916(11)	3.686109(13)
Γ_{ee} (keV)	5.55(14)	2.37(4)
$(\alpha/\alpha(M))^2$	0.9580(3)	0.9557(6)

Table 6. Masses and electronic widths [65] of the narrow charmonium resonances with total uncertainties and effective electromagnetic coupling, where $\alpha = 1/137.035999084(51)$ is the fine structure constant, and $\alpha(M)$ stands for the pole-subtracted effective electromagnetic coupling at the scale M [66]. We have also given the uncertainties in $\alpha(M)$ due to its hadronic contributions. Compared to the uncertainties of the widths, the uncertainties on $\alpha(M)$ and the masses are negligible.

3 Experimental Data

3.1 Data Collections

Narrow resonances

Below the open charm threshold there are the J/ψ and ψ' narrow charmonium resonances. Their masses, and electronic widths are taken from the PDG [65]¹³ and are collected in Tab. 6 together with the value of the pole-subtracted effective electromagnetic coupling at their masses. The total widths are not relevant since we use the narrow width approximation for their contributions to the moments. The uncertainty for the contribution to the moments coming from the masses and the effective electromagnetic coupling can be neglected.

Threshold and data continuum region

The open charm threshold is located at $\sqrt{s} = 3.73\text{ GeV}$. We call the energies from just

¹³We actually use the most up to date values corresponding to: J. Beringer et al. (Particle Data Group), Phys. Rev. D86, 010001 (2012) and 2013 partial update for the 2014 edition.

below the threshold and up to 5 GeV the threshold region, and the region between 5 GeV and 10.538 GeV, where the production rate is dominated by multiparticle final states the data continuum region. In these regions quite a variety of measurements of the total hadronic cross section exist from BES [20–25], CrystalBall [26, 27], CLEO [28–31], MD1 [32], PLUTO [33], and MARKI and II [34–37]. Taken together, the entire energy region up to 10.538 GeV is densely covered with total cross section measurements from these 19 data sets.¹⁴ The measurements from BES and CLEO have the smallest uncertainties. They do, however, not cover the region between 5 and 7 GeV. Here CrystalBall and MARKI and II have contributed measurements albeit with somewhat larger uncertainties. The statistical and total systematical uncertainties of the measurements can be extracted from the respective publications. For some data sets the amount of uncorrelated and correlated systematical uncertainties is given separately (BES [21, 23, 24], CrystalBall [26, 27], CLEO [30], MARKI and II [36, 37], MD1 [32]) while for all the other data sets only combined systematical uncertainties are quoted. All these data sets are shown in Figs. 8, where the displayed error bars represent the (quadratically) combined statistical and systematical uncertainties.

Interestingly, none of the previous charm mass analyses, to the best of our knowledge, ever used the complete set of available data. As examples, Bodenstein et al. [67] used data sets [20, 21, 24, 31] from BES and CLEO. Jamin and Hoang [38] used the data sets of Refs. [21], [32] and [28] from BES, MD1 and CLEO, covering the regions $2 \text{ GeV} \leq E \leq 4.8 \text{ GeV}$ and $6.964 \text{ GeV} \leq E \leq 10.538 \text{ GeV}$. Boughezal et al. [13], Kuhn et al. [5], and Narison [68] use only one data set from BES [21]. Kuhn et al. [39, 40] used the data sets of Refs. [21, 24] from BES covering the energy region $2.6 \text{ GeV} \leq E \leq 4.8 \text{ GeV}$.

We consider three different selections of data sets to study the dependence of the experimental moments on this choice:

1. The *minimal selection* contains all data sets necessary to cover the whole energy region between 2 and 10.538 GeV without any gaps and keeping only the most accurate ones. These 8 data sets are from BES [20, 21, 23, 25], CrystalBall [27], CLEO [30, 31] and MD1 [32] corresponding to the data sets 1, 2, 5, 6, 9, 12, 13, and 14 (see Tab. 7 for references).
2. The *default selection* contains all data sets except for the three ones with the largest uncertainties. It contains 16 data sets and fully includes the minimal selection. It contains all data sets except for Mark I and II data sets 16, 17 and 19 from Refs. [34, 35, 37].
3. The *maximal selection* contains all 19 data sets.

We use the default selection as our standard choice for the charm mass analysis, but we will also quote results for the other data selections.

Perturbative QCD region

¹⁴There are 18 references quoted since Ref. [27] provides results from two independent runs that we treat as two different data sets.

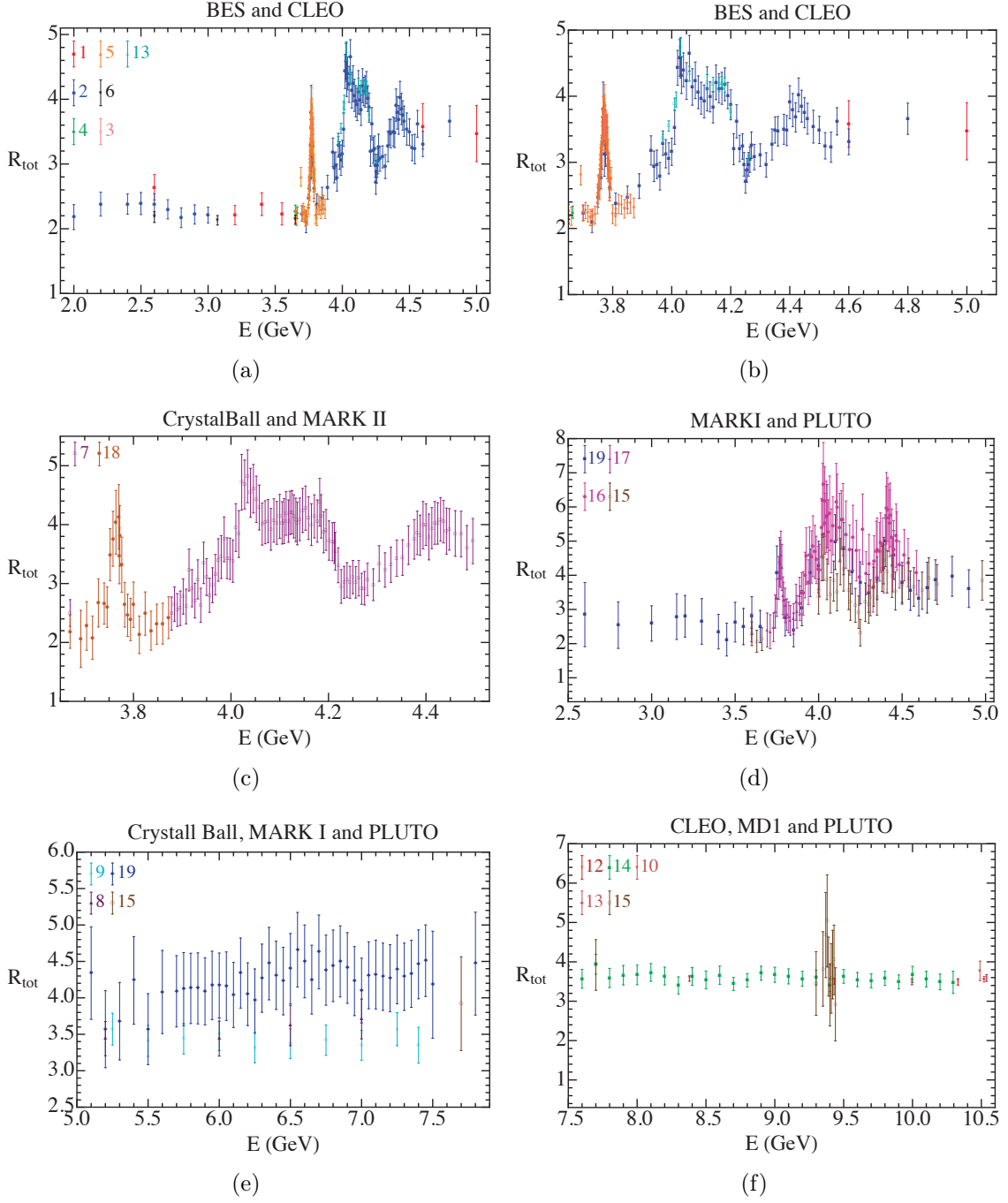


Figure 8. Experimental data. In the two top figures we show BES and CLEO data in the non-charm, low charm and threshold regions (a) and low charm region and threshold region (b). The two pictures in the middle show less precise data in the threshold region: CrystalBall and MARKII (c) and MARKI and PLUTO (d). The two pictures on the bottom show data in the continuum region: below 8 GeV data from CrystalBall, MARKI and PLUTO (e) and above 8 GeV data from CLEO, MD1 and PLUTO (f).

Numbering	Reference	Experiment	Year	Systematical	Data points
1	[20]	BES	2000	no splitting given	6
2	[21]	BES	2002	splitting given	85
3	[22]	BES	2004	only one point	1
4	[23]	BES	2006	splitting given	3
5	[24]	BES	2006	splitting given	68
6	[25]	BES	2009	no splitting given	3
7	[26]	CrystalBall	1986	splitting given	98
8	[27]	CrystalBall (Run 1)	1990	splitting given	4
9	[27]	CrystalBall	1990	splitting given	11
10	[28]	CLEO	1979	only one point	1
11	[29]	CLEO	1998	only one point	1
12	[30]	CLEO	2007	splitting given	7
13	[31]	CLEO	2008	no splitting given	13
14	[32]	MD1	1996	splitting given	31
15	[33]	PLUTO	1982	no splitting given	45
16	[34]	MARKI	1976	no splitting given	59
17	[35]	MARKI	1977	no splitting given	21
18	[36]	MARKII	1979	splitting given	24
19	[37]	MARKI	1981	splitting given	78

Table 7. Complete data set of measurements of the total hadronic R -ratio used in this work. Each data set is assigned a number to simplify referencing in discussions and figures of this work. Also given is information on the name of the experimental collaboration, the year of the publication, on whether the splitting of the systematical error in correlated and uncorrelated contributions is provided, and on the number of data points.

Above 10.538 GeV there are no experimental measurements of the total hadronic R -ratio that might be useful for the experimental moments. In this energy region we will therefore use perturbative QCD to provide estimates for the charm production R -ratio. As a penalty for not using experimental data we assign a 10% total relative uncertainty to the contribution of the experimental moments coming from this region, which we then treat like an uncorrelated experimental uncertainty for the combination with the moment contribution from lower energies. We stress that this error is not related to the theoretical uncertainty of perturbative QCD in this region (which amounts to less than 0.5%), but represents a conservative error assignment that allows to trace the impact of this region in the analyses. We have fixed the value of 10% as twice the overall offset between the combined data and the perturbative QCD prediction for the charm cross section in the energy region between

4.55 and 10.538 GeV, see the discussion at the end of Sec. 3.2. As we see in Sec. 3.3 the energy region above 10.538 GeV contributes only (6, 0.4, 0.03, 0.002)% to $M_{1,2,3,4}^{\text{exp}}$. In the first moment M_1^{exp} the total contribution is about three times larger than the combined statistical and systematical (true) experimental uncertainties from the other energy regions. So the 10% penalty we assign to this approach represents a subleading component of the final quoted uncertainty.¹⁵ In the second and higher moments $M_{n \geq 2}^{\text{exp}}$ the contributions from above 10.538 GeV and the corresponding uncertainty are negligible compared to the uncertainties from the lower energy regions. This means that our experimental moments are completely free from any theory-driven input or potential bias.

As the theoretical formula to determine the moment contribution from the perturbative QCD region we use the $\mathcal{O}(\alpha_s)$ [6], $\mathcal{O}(\alpha_s^2)$ [69–71], and $\mathcal{O}(\alpha_s^3)$ [72, 73] nonsinglet massless quark cross section including charm mass corrections up to $\mathcal{O}(\bar{m}_c^4/s^2)$ [74–78]:

$$R_{cc}^{\text{th}}(s) = N_c Q_c^2 R^{\text{ns}}(s, \bar{m}_c^2(\sqrt{s}), n_f = 4, \alpha_s^{n_f=4}(\sqrt{s}), \sqrt{s}), \quad (3.1)$$

where

$$\begin{aligned} R^{\text{ns}}(s, \bar{m}_c^2(\sqrt{s}), n_f = 4, \alpha_s^{n_f=4}(\sqrt{s}), \sqrt{s}) \\ = 1 + \frac{\alpha_s}{\pi} + 1.52453 \left(\frac{\alpha_s}{\pi} \right)^2 - 11.52034 \left(\frac{\alpha_s}{\pi} \right)^3 \\ + \frac{\bar{m}_c^2(\sqrt{s})}{s} \left[12 \frac{\alpha_s}{\pi} + 109.167 \left(\frac{\alpha_s}{\pi} \right)^2 + 634.957 \left(\frac{\alpha_s}{\pi} \right)^3 \right] \\ + \frac{\bar{m}_c^4(\sqrt{s})}{s^2} \left[-6 - 22 \frac{\alpha_s}{\pi} + 140.855 \left(\frac{\alpha_s}{\pi} \right)^2 + \left(\frac{\alpha_s}{\pi} \right)^3 (3776.94 + 10.3333 L_m^2) \right], \end{aligned} \quad (3.2)$$

with

$$L_m \equiv \ln \left(\frac{\bar{m}_c^2(\sqrt{s})}{s} \right). \quad (3.3)$$

For the computation of the contribution to the experimental moments we determine $\bar{m}_c(\sqrt{s})$ and $\alpha_s(\sqrt{s})$ appearing in Eq. (3.1) using $\bar{m}_c(\bar{m}_c) = 1.3$ GeV and $\alpha_s(m_Z) = 0.118$ as initial conditions.

It is instructive to examine for the moment contributions from $\sqrt{s} > 10.538$ GeV terms related to charm production that we do not account for in Eq. (3.2). In Tab. 8 the relative size with respect to the full first four moments (in percent) of the most important neglected contributions are given. In the second column the size of the mass corrections up to order \bar{m}_c^4 , which we have included in R_{cc}^{th} , are shown as a reference. The third column shows the contributions coming from secondary $c\bar{c}$ radiation through gluon splitting. The fourth column depicts the contributions from the $\mathcal{O}(\alpha_s^3)$ singlet corrections (including the mass corrections up to order \bar{m}_c^4), which one can take as an rough estimate for the actual contributions from the charm cut. Finally in the last column we show the size of the Z-boson exchange terms integrated from threshold to 10.538 GeV. This contribution represents the

¹⁵ The situation is quite different if experimental data from the region above 4.8 GeV is discarded and perturbative QCD is used already from 4.8 GeV. Here the contribution to the moments $M_{1,2,3,4}^{\text{exp}}$ from energies above 4.8 GeV amounts to (30, 10, 3, 1)%. For the first moment the 10% penalty would then represent the largest source of uncertainty and correspond to an uncertainty in the charm mass of around 18 MeV.

n	Mass corrections	Secondary Radiation	Singlet	Z-boson
1	0.02	0.038	3×10^{-4}	0.006
2	0.001	9×10^{-4}	2×10^{-5}	0.004
3	1×10^{-4}	4×10^{-5}	2×10^{-6}	0.003
4	8×10^{-6}	3×10^{-6}	1×10^{-7}	0.003

Table 8. Relative size (in percent) of some subleading contributions for the first four moments originating from energies $\sqrt{s} > 10.538$ GeV. The second column shows the charm mass corrections contained in R_{cc}^{th} as a reference. The third column shows the contributions from $\mathcal{O}(\alpha_s^2)$ secondary $c\bar{c}$ radiation through gluon splitting. The effects from secondary charm radiation accounting all energies from threshold to infinity are $(0.042, 0.002, 3 \times 10^{-4}, 7 \times 10^{-5})\%$ for the first four moments. The fourth column depicts the contribution from the $\mathcal{O}(\alpha_s^3)$ singlet gluon corrections accounting for the mass corrections up to order \bar{m}_c^4 . Integrating the known singlet corrections from threshold to infinity the contributions amount to $(0.005, 0.003, 0.002, 0.001)\%$ for the first four moments. The last column shows the relative corrections from the Z-boson exchange integrated from threshold to 10.538 GeV.

Z-exchange contribution that is contained in the data, but - by definition - not accounted for in the theory moments. We see that at least for the first two moments, the contributions neglected are much smaller than the charm mass corrections we have accounted for in the nonsinglet production rate, which are already constituting a very small effect. Overall the numerical effect on the charm mass of all these contributions is tiny considering the scaling $\bar{m}_c \sim M_n^{1/2n}$. Since we assign a 10% error on the moments' contribution from the energy region $\sqrt{s} > 10.538$ GeV where we use theory input, our approach to neglect subleading effects is justified.

Non-charm background

Experimentally only the total hadronic cross section is available. Although charm-tagged rate measurements are in principle possible [31] they have not been provided in publications. On the other hand, they would also exhibit sizable additional uncertainties related to the dependence on simulations of the decay of charmed mesons into light quark final states. So to obtain the charm production cross section from the data we have to subtract the non-charm background using a model based on perturbative QCD related to the production of u , d and s quarks. A subtle point is related to the secondary radiation of $c\bar{c}$ pairs off the u , d and s quarks from gluon splitting and to which extent one has to account theoretically for the interplay between real and virtual secondary $c\bar{c}$ radiation which involves infrared sensitive terms [79]. Since in this work we define the moments from primary $c\bar{c}$ production (see Eq. (1.1)), secondary $c\bar{c}$ production is formally counted as non-charm background.

Thus for the model for the non-charm background for $\sqrt{s} > 2\bar{m}_c$ we employ the expression

$$R_{uds}(s) = N_c(Q_u^2 + 2Q_d^2) \left[R^{\text{ns}}(s, 0, n_f = 3, \alpha_s^{n_f=4}(\sqrt{s}), \sqrt{s}) \right. \\ \left. + \left(\frac{\alpha_s^{n_f=4}(\sqrt{s})}{\pi} \right)^2 \frac{2}{3} \left(\rho^V + \rho^R + \frac{1}{4} \log \frac{\bar{m}_c^2(\bar{m}_c)}{s} \right) \right]. \quad (3.4)$$

The second term on the RHS describes the contributions from real and virtual secondary $c\bar{c}$ radiation. The analytic expressions for ρ^R and ρ^V can be found in Eqs. (2) and (6) of Ref. [80]. We have checked that the numerical impact of real (ρ^R) and virtual (ρ^V) secondary radiation individually as well as the complete second term on the RHS of Eq. (3.4) on the moments is negligible, see Tab. 8. We use Eq. (3.4) and fit the non-charm background including also data in the region $2 \text{ GeV} \leq E \leq 3.73 \text{ GeV}$ via the ansatz $R_{\text{non-}c\bar{c}}(s) = n_{\text{ns}} R_{uds}(s)$, where the constant n_{ns} represents an additional fit parameter. We determine n_{ns} from a global combined fit including many data sets, as explained below. This is similar in spirit to Refs. [40], where an analogous constant n_- was determined. Their approach, however, differs from ours as they fitted n_- separately for the two considered BES data sets [21] and [24] accounting only energies below 3.73 GeV.

3.2 Data Combination

Combining different experimental measurements of the hadronic cross section one has to face several issues: (a) the measurements are given at individual separated energy points, (b) the set of measurements from different publications are not equally spaced, cover different, partly overlapping energy regions and have different statistical and systematical uncertainties, (c) the correlations of systematical errors are only known (or provided) for the data sets within each publication, (d) there are a number of very precise measurements at widely separated energies.

In this section we discuss the combination of the experimental data from the threshold and the data continuum regions between 2 and 10.538 GeV using a method based on a fitting procedure used before for determining the hadronic vacuum polarization effects for $g-2$ [48]. In this work we extend this approach and also account for the subtraction of the non-charm background.

Combination method

The method uses the combination of data in energy bins (clusters) assuming that the R -value within each cluster changes only very little and can thus be well approximated by a constant. Thus clusters for energies where R varies rapidly need to be small (in this case the experimental measurements are also denser). The R -value in each cluster is then obtained by a χ^2 fitting procedure. Since each experimental data set from any publication covers an energy range overlapping with at least one other data set, the clusters are chosen such that clusters in overlapping regions contain measurements from different data sets. Through the fitting procedure correlations are then being communicated among different data sets and very accurate individual measurements can inherit their precision into neighboring clusters.

Both issues are desirable since the hadronic R -ratio is a smooth function with respect to the sequence of clusters.

To describe the method we have to set up some notation:

- All measurements $R(E)$ are distinguished according to the energy E at which they have been carried out.
- Each such energy point having a measurement is written as $E_i^{k,m}$, where $k = 1, \dots, N_{\text{exp}}$ refers to the N_{exp} data sets, $m = 1, \dots, N_{\text{cluster}}$ runs over the N_{cluster} clusters and $i = 1, \dots, N^{k,m}$ assigns the i -th of the $N^{k,m}$ measurements.
- Each individual measurement of the R -ratio is then written as

$$R(E_i^{k,m}) = R_i^{k,m} \pm \sigma_i^{k,m} \pm \Delta_i^{k,m}, \quad (3.5)$$

where $R_i^{k,m}$ is the central value, $\sigma_i^{k,m}$ the combined statistical and uncorrelated systematical uncertainty and $\Delta_i^{k,m}$ the correlated systematical experimental uncertainty.

- For convenience we define $\Delta f_i^{k,m} = \Delta_i^{k,m}/R_i^{k,m}$ to be the relative systematical correlated uncertainty.

As our standard choice concerning the clusters we use 5 different regions each having equidistant cluster sizes ΔE . The regions are as follows:

- (0) **non-charm region**: has 1 cluster for $2 \text{ GeV} \leq E \leq 3.73 \text{ GeV}$ ($\Delta E = 1.73 \text{ GeV}$).
- (1) **low charm region**: has 2 clusters for $3.73 \text{ GeV} < E \leq 3.75 \text{ GeV}$ ($\Delta E = 10 \text{ MeV}$).
- (2) **$\psi(3S)$ region/threshold region 1**: has 20 cluster for $3.75 \text{ GeV} < E \leq 3.79 \text{ GeV}$ ($\Delta E = 2 \text{ MeV}$).
- (3) **resonance region 2**: has 20 cluster for $3.79 \text{ GeV} < E \leq 4.55 \text{ GeV}$ ($\Delta E = 38 \text{ MeV}$).
- (4) **continuum region**: has 10 cluster for $4.55 \text{ GeV} < E \leq 10.538 \text{ GeV}$ ($\Delta E = 598.8 \text{ MeV}$).

We assign to this choice of $52 + 1$ clusters the notation (2,20,20,10) and later also examine alternative cluster choices demonstrating that the outcome for the moments does within errors not depend on them. The cluster in the non-charm region is used to fit for the normalization constant n_{ns} of the non-charm background contribution, see Eq. (3.4).

Our standard procedure to determine the central energy E_m associated to each cluster is just the weighted average of the energies of all measurements falling into cluster m ,

$$E_m = \frac{\sum_{k,i} \frac{E_i^{k,m}}{(\sigma_i^{k,m})^2 + (\Delta_i^{k,m})^2}}{\sum_{k,i} \frac{1}{(\sigma_i^{k,m})^2 + (\Delta_i^{k,m})^2}}. \quad (3.6)$$

The corresponding R -value for the charm cross section that we determine through the fit procedure described below is called

$$R_m \equiv R_{c\bar{c}}(E_m). \quad (3.7)$$

We note that using instead the unweighted average or simply the center of the cluster has a negligible effect on the outcome for the moments since the clusters we are employing are sufficiently narrow.

Fit procedure and χ^2 -function

We determine the charm cross section $R_{c\bar{c}}$ from a χ^2 -function that accounts for the positive correlation among the systematical uncertainties $\Delta_i^{k,m}$ within each experiment k and, at the same time, also for the non-charm background. To implement the correlation we introduce the auxiliary parameters d_k ($k = 1, \dots, N_{\text{exp}}$) that parametrize the correlated deviation from the experimental central values $R_i^{k,m}$ in units of the correlated systematical uncertainty $\Delta_i^{k,m}$, see Eq. (3.5). In this way we carry out fits to $R_i^{k,m} + d_k \Delta_i^{k,m}$ and treat the d_k as additional auxiliary fit parameters that are constraint to be of order one (one standard deviation) by adding the term

$$\chi_{\text{corr}}^2(\{d_k\}) = \sum_{k=1}^{N_{\text{exp}}} d_k^2, \quad (3.8)$$

to the χ^2 -function. To implement the non-charm background we assume that the relative energy dependence of the non-charm cross section related to primary production of u , d and s quarks is described properly by R_{uds} given in Eq. (3.4). We then parametrize the non-charm background cross section by the relation

$$R_{\text{non-}c\bar{c}}(E) = n_{\text{ns}} R_{uds}(E) \quad (3.9)$$

as already described in Sec. 3.1, where the fit parameter n_{ns} is determined mainly from the experimental data in the first clusters below 3.73 GeV by adding the term

$$\chi_{\text{nc}}^2(n_{\text{ns}}, \{d_k\}) = \sum_{k=1}^{N_{\text{exp}}} \sum_{i=1}^{N^{k,1}} \left(\frac{R_i^{k,1} - (1 + \Delta f_i^{k,1} d_k) n_{\text{ns}} R_{uds}(E_i^{k,1})}{\sigma_i^{k,1}} \right)^2, \quad (3.10)$$

to the χ^2 -function. The complete χ^2 -function then has the form

$$\chi^2(\{R_m\}, n_{\text{ns}}, \{d_k\}) = \chi_{\text{corr}}^2(\{d_k\}) + \chi_{\text{nc}}^2(n_{\text{ns}}, \{d_k\}) + \chi_c^2(\{R_m\}, n_{\text{ns}}, \{d_k\}), \quad (3.11)$$

where¹⁶

$$\chi_c^2(\{R_m\}, n_{\text{ns}}, \{d_k\}) = \sum_{k=1}^{N_{\text{exp}}} \sum_{m=2}^{N_{\text{clusters}}} \sum_{i=1}^{N^{k,m}} \left(\frac{R_i^{k,m} - (1 + \Delta f_i^{k,m} d_k) (R_m + n_{\text{ns}} R_{uds}(E_i^{k,m}))}{\sigma_i^{k,m}} \right)^2. \quad (3.12)$$

¹⁶We have checked that the effect of using $R_{uds}(E_m)$ instead of $R_{uds}(E_i^{k,m})$ is totally negligible.

Note that in our approach the non-charm normalization constant n_{ns} is obtained from a combined fit together with the cluster values R_m .

This form of the χ^2 -function is an extended and adapted version of the ones used in Refs. [46, 47]. A special characteristic of the χ^2 -functions in Eqs. (3.10) and (3.12) is that the relative correlated experimental uncertainties $\Delta f_i^{k,m}$ enter the χ^2 -function by multiplying the fit value R_m rather than the experimental values $R_i^{k,m}$. This leads to a non-bilinear dependence of the χ^2 -function on the d_m and the R_m fit parameters and avoids spurious solutions where the best fit values for the R_m are located systematically below the measurements. Such spurious solutions can arise for data points with substantial positive correlation when χ^2 -functions with strictly bilinear dependences are employed [46, 47].¹⁷

We also note that the implementation of the non-charm background subtraction given in Eq. (3.12) leads to a partial cancellation of systematical uncertainties for the R_m best fit values for the charm cross section. Moreover, it is interesting to mention that in the limit where each cluster contains exactly one measurement (except below threshold, in which we always keep one cluster) the χ^2 -function decouples, after performing the change of variables $R'_m = R_m + n_{\text{ns}} R_{uds}(E^{k,m})$, into the sum of two independent χ^2 -functions, one containing data below threshold and depending only on n_{ns} and d_k , and another one containing data above threshold $R^{k,m}$ (we drop the label i because having only one data per cluster it can take only the value 1) and depending only on R'_m . After minimizing the first χ^2 -function one can obtain the best fit values for n_{ns} and d_k , denoted by $n_s^{(0)}$ and $d_k^{(0)}$, respectively. The second χ^2 has a minimal value of 0 and the best fit parameters read $R_m^{(0)} = R^{k,m} / (1 + d_k^{(0)} \Delta^{k,m}) - n_{\text{ns}}^{(0)} R_{uds}(E^{k,m})$.

Close to the minimum the χ^2 -function of Eq. (3.11) can be written in the Gaussian approximation

$$\chi^2(\{p_i\}) = \chi_{\text{min}}^2 + \sum_{i,j} (p_i - p_i^{(0)}) V_{i,j}^{-1} (p_j - p_j^{(0)}) + \mathcal{O}((p - p^{(0)})^3), \quad (3.13)$$

where $p_i = (\{R_m\}, n_{\text{ns}}, \{d_k\})$ and the superscript (0) indicates the respective best fit value. After determination of the correlation matrix V_{ij} by numerically inverting $V_{i,j}^{-1}$ we can drop the dependence on the auxiliary variables n_{nc} and d_k and obtain the correlation matrix of the R_m from the R_m -submatrix of V_{ij} which we call $V_{mm'}^R$. In order to separate uncorrelated statistical and systematical uncertainties from correlated systematical ones we compute the complete $V_{mm'}^R$ accounting for all uncertainties and a simpler version of the correlation matrix, $V_{mm'}^{R,u}$ accounting only for uncorrelated uncertainties. The latter is obtained from dropping all correlated errors $\Delta_i^{k,m}$ from the χ^2 -function (3.11).¹⁸

The outcome of the fit for the sum of the charm and the non-charm cross section in the threshold and the data continuum region using the standard data set explained above is shown in Figs. 9(a)-(f) together with the input data sets. The red line segments connect the

¹⁷ We prove in Appendix B the equivalence of a bilinear χ^2 -function with fit auxiliary parameters to a bilinear χ^2 -function without auxiliary fit parameters, but containing the standard correlation matrix.

¹⁸ In a very good approximation, it can be also obtained by dropping in $V_{i,j}^{-1}$ the rows and columns corresponding to d_k and inverting the resulting matrix. After that one also drops the row and column corresponding to n_{nc} . We adopt this simplified procedure for our numerical fits.

best fit values and the brown band represents the combined total uncertainty. The clusters are indicated by dashed vertical lines. For completeness we have also given all numerical results for the R_m values in Appendix A. There we also give results for the minimal and maximal data set selections.

The fit results in the continuum region for the energies between 4.55 GeV and 10.538 GeV allow for an interesting comparison of the R -values obtained from perturbative QCD and from experimental data based on our combined fit procedure. In the left panel of Fig. 10 the fit results for the charm cross section are shown together with the perturbative QCD prediction from Eq. (3.2) (black solid line). Within the total experimental errors, which are around 5%, there is good agreement between data and the perturbative QCD result (which itself has a perturbative error due to scale variations of less than 1%). Interestingly, there appears to be some oscillatory behavior of the data around the perturbative QCD result, although the statistical power of the data is insufficient to draw definite conclusions concerning the physics of these oscillations. Concerning the contributions to the moments we find $M_{1,\text{ex}}^{(4.55-10.538)\text{GeV}} = 4.81 \pm 0.18$ from the data compared to $M_1^{(4.55-10.538)\text{GeV}} = 5.010 \pm 0.011$ from perturbative QCD based on Eq. (3.2). The central value from perturbative QCD is 4% above the experimental moment. This shows that adopting perturbative QCD predictions instead of data gives a contribution to the central value of the moments compatible within the experimental uncertainties. However, using theoretical uncertainties as an estimate for the experimental ones leads to an underestimate. In the right panel of Fig. 10 the experimental data and the perturbative QCD predictions are compared for the total hadronic cross section. Here the perturbative QCD result is shifted downward with respect to the data due to the non-charm normalization constant n_{ns} obtained from our combined fit being slightly larger than unity, see Eq. (A.2). Overall, the agreement between the combined data and perturbative QCD appears to be even better than for the charm cross section in particular for the energy region above 9 GeV.

3.3 Experimental Moments

Narrow resonances

For the J/ψ and ψ' charmonium contributions to the experimental moments we use the narrow width approximation,

$$M_n^{\text{res}} = \frac{9 \pi \Gamma_{ee}}{\alpha(M)^2 M^{2n+1}}, \quad (3.14)$$

with the input numbers given in Tab. 6. We neglect the tiny uncertainties in the charmonium masses as their effects are negligible.

Threshold and data continuum region

For the determination of the moment contributions from the threshold and the continuum region between 3.73 and 10.538 GeV we use the results for the clustered $c\bar{c}$ cross section values R_m determined in Sec. 3.2 and the trapezoidal rule. We employ a linear interpolation for the cross section but keep the analytic form of the integration kernel $1/s^{n+1}$ exact by

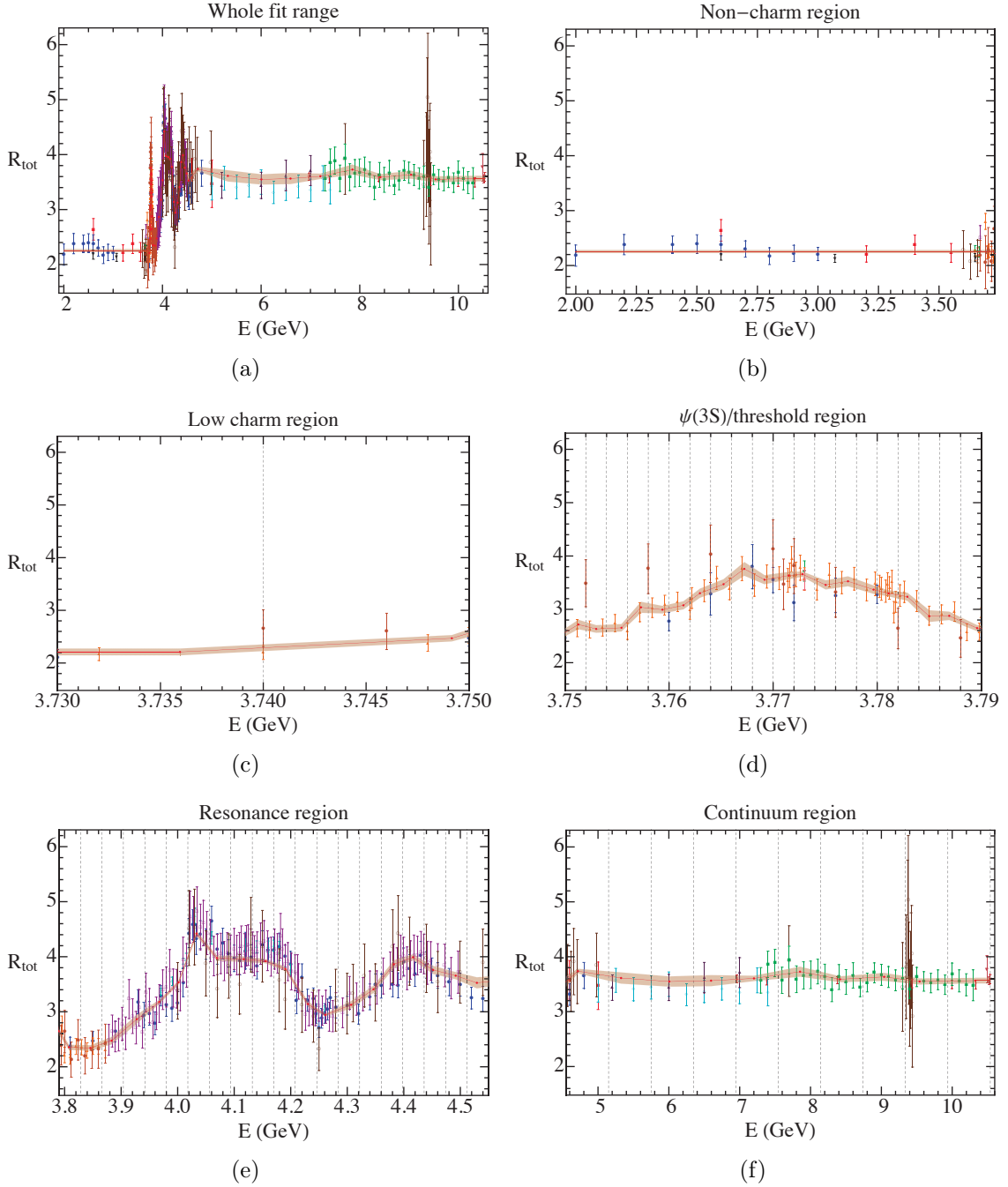


Figure 9. Result of the fit for the default selection of data sets. On the top, (a) and (b) show the entire fit region and the non-charm region, respectively. In the middle row, (c) illustrates the low charm region and (d) the threshold region 1. In the bottom line (e) and (f) depict threshold region 2 and the data continuum region, respectively.

including it into the integration measure. Using the relation $ds/s^{n+1} = d(E^{-2n}/n)$ we thus

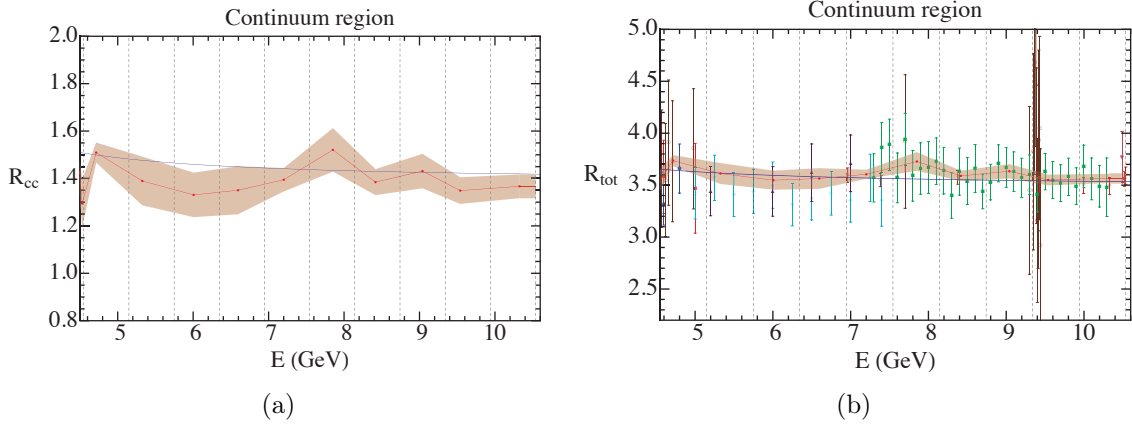


Figure 10. Comparison of experimental data (red dots) with uncertainties (brown error band) and the predictions from perturbative QCD (black solid line) for the charm cross section $R_{c\bar{c}}$ (left panel) and the total cross section R_{tot} (right panel).

obtain

$$M_n^{\text{thr+cont}} = \frac{1}{2n} \left[\sum_{i=1}^{N_{\text{clusters}}} R_i \left(\frac{1}{E_{i-1}^{2n}} - \frac{1}{E_{i+1}^{2n}} \right) + R_0 \left(\frac{1}{E_0^{2n}} - \frac{1}{E_1^{2n}} \right) \right. \\ \left. + R_{N_{\text{clusters}}+1} \left(\frac{1}{E_{N_{\text{clusters}}}^{2n}} - \frac{1}{E_{N_{\text{clusters}}+1}^{2n}} \right) \right], \quad (3.15)$$

where R_0 and E_0 are the R and energy values at the lower boundary of the smallest energy cluster, and $R_{N_{cl}+1}$ and $E_{N_{cl}+1}$ are the corresponding values of the upper boundary of the highest energy cluster. The values for R_0 and $R_{N_{cl}+1}$ are obtained from linear extrapolation using the R_m values of the two closest lying clusters¹⁹ m' and $m' + 1$ with the formula

$$R(E) = \frac{R_{m'+1} - R_{m'}}{E_{m'+1} - E_{m'}} (E - E_{m'}) + R_{m'}. \quad (3.16)$$

For the computation of the moment contributions from subintervals within the range between 3.73 and 10.538 GeV we also use Eq. (3.15) using corresponding adaptations for the boundary values at $m = 0$ and $m = N_{cl} + 1$.

Perturbative QCD region

For the region above 10.538 GeV where we use the perturbative QCD input described in Eqs. (3.1) and (3.2) for the charm R -ratio the contribution to the experimental moment is obtained from the defining equation (1.2) with a lower integration limit of 10.538 GeV:

$$M_n^{\text{QCD}} = \gamma \times \int_{(10.538 \text{ GeV})^2}^{\infty} ds \frac{R_{cc}^{\text{th}}(s)}{s^{n+1}}. \quad (3.17)$$

The variable γ is an auxiliary variable used to parametrize the 10% uncertainty we assign to the perturbative QCD contribution,

$$\gamma = 1.0 \pm 0.1. \quad (3.18)$$

¹⁹ For R_0 we have $m' = 1$ and for $R_{N_{cl}+1}$ we have $m' = N_{cl} - 1$.

Correlations

The experimental moments are obtained from the sum of the resonance, threshold plus continuum and perturbative QCD contributions described just above,

$$M_n^{\text{exp}} = M_n^{\text{res}} + M_n^{\text{thr+cont}} + M_n^{\text{QCD}}. \quad (3.19)$$

To determine the uncertainties we account for the errors in the e^+e^- widths of J/ψ and ψ' and in the cluster values R_m , and for the 10% assigned uncertainty in M_n^{QCD} . For the evaluation we use the usual error propagation based on a $\bar{m} \times \bar{m}$ correlation matrix with $\bar{m} = N_{cl} + 3$. The correlation matrix of the experimental moments thus has the form

$$C_{nn'}^{\text{exp}} = \sum_{i,j=1}^{N_{cl}+3} \left(\frac{\partial M_n^{\text{exp}}}{\partial \bar{R}_i} \right) \left(\frac{\partial M_{n'}^{\text{exp}}}{\partial \bar{R}_j} \right) V_{ij}^{\bar{R}}, \quad (3.20)$$

where we have $\bar{R}_i = (\{R_m\}, \Gamma_{e^+e^-}(J/\psi), \Gamma_{e^+e^-}(\psi'), \gamma)$. The entries of $V^{\bar{R}}$ in the R_m subspace are just the entries of the correlation matrix V^R obtained from the cluster fit. The diagonal entries in the $\Gamma_{e^+e^-}$ subspace are the combined statistical and systematical uncertainties of the e^+e^- widths and the $\delta\gamma = 0.1$ for M_n^{QCD} , respectively. We treat the latter uncertainty as uncorrelated with all other uncertainties. So all non-diagonal entries of $V_{ij}^{\bar{R}}$ for i or $j = N_{cl} + 3$ are zero. For the uncertainty of the e^+e^- widths we adopt a model where the (quadratic) half of the error is uncorrelated and the other (quadratic) half is positively correlated among the two narrow resonances, while we assume no correlation between the narrow resonances and the R_n cluster values.²⁰ Thus for the corresponding non-diagonal entries of $V_{i,j}^{\bar{R}}$ with $i \in \{1, N_{cl}\}$ and $j = \{N_{cl} + 1, N_{cl} + 2\}$ we have the entries $V_{ij}^{\bar{R}} = 0$, and for $i = N_{cl} + 1$ and $j = N_{cl} + 2$ we have $V_{ij}^{\bar{R}} = \delta\Gamma_{e^+e^-}^1 \delta\Gamma_{e^+e^-}^2 / 2$, where $\delta\Gamma_{e^+e^-}^{1,2}$ are the respective e^+e^- width total uncertainties for J/ψ and ψ' , respectively.

The results for the moments showing separately the contributions from the resonances, various energy subintervals and their total sum using the defaults data set collection (see Sec. 3.1) are given in Tab. 9. Using Eq. (3.20) it is straightforward to compute the correlation matrix of the moments, and we obtain

$$C^{\text{exp}} = \begin{pmatrix} 0.128 & 0.084 & 0.077 & 0.075 \\ 0.084 & 0.076 & 0.074 & 0.075 \\ 0.077 & 0.074 & 0.075 & 0.077 \\ 0.075 & 0.075 & 0.077 & 0.079 \end{pmatrix}, \quad (3.21)$$

for the total correlation matrix accounting for all correlated and uncorrelated uncertainties. We remind the reader that all numbers related to the moment M_n^{exp} are given in units of $10^{-(n+1)} \text{ GeV}^{-2n}$. To quote correlated and uncorrelated uncertainties separately it is also useful to show the correlation matrix that is obtained when only uncorrelated uncertainties

²⁰We thank J. J. Hernández Rey for pointing out that, although a coherent study of these correlations does not exist, treating resonances as uncorrelated to the continuum represents the most appropriate correlation model.

n	Resonances	3.73 – 4.8	4.8 – 7.25	7.25 – 10.538	10.538 – ∞	Total
1	11.91(17 20)	3.23(4 6)	3.39(8 13)	1.42(2 5)	1.27(0 13)	21.21(20 30)
2	11.68(18 20)	1.78(2 3)	1.06(3 4)	0.200(3 7)	0.057(0 6)	14.78(18 21)
3	11.63(18 20)	1.00(1 2)	0.350(9 13)	0.0294(6 10)	0.0034(0 3)	13.02(19 20)
4	11.73(19 20)	0.571(7 11)	0.121(3 4)	0.00448(9 15)	$2.3(0 2) \times 10^{-4}$	12.43(19 20)

Table 9. Result for the experimental moments for the standard selection of data sets. The second column collects the contribution from the narrow resonances J/ψ and ψ' treated in the narrow width approximation. Third to fifth columns are shown only as an illustration, but use the outcome of the fit to the entire fit region, 3.73 – 10.538 GeV. The sixth column is obtained using perturbation theory, and the last column shows the number for the complete moment. For the moment M_n^{exp} all numbers are given in units of $10^{-(n+1)} \text{ GeV}^{-2n}$.

n	Resonances	3.73 – 4.8	4.8 – 7.25	7.25 – 10.538	10.538 – ∞	Total
1	11.91(17 20)	3.14(6 8)	3.24(9 16)	1.38(2 6)	1.27(0 13)	20.95(21 33)
2	11.68(18 20)	1.75(3 4)	1.01(3 5)	0.195(4 9)	0.057(0 6)	14.69(18 21)
3	11.63(18 20)	0.99(2 3)	0.33(1 2)	0.0287(6 12)	0.0034(0 3)	12.99(19 20)
4	11.73(19 20)	0.57(1 1)	0.114(4 5)	0.0044(1 2)	$2.3(0 2) \times 10^{-4}$	12.42(19 20)

Table 10. Results for the experimental moments for the minimal selection of data sets. Conventions are as in Tab. 9. All moments are given in units of $10^{-(n+1)} \text{ GeV}^{-2n}$.

n	Resonances	3.73 – 4.8	4.8 – 7.25	7.25 – 10.538	10.538 – ∞	Total
1	11.91(17 20)	3.19(3 5)	3.60(6 6)	1.54(2 4)	1.27(0 13)	21.50(19 27)
2	11.68(18 20)	1.77(2 3)	1.11(2 2)	0.217(4 5)	0.057(0 6)	14.83(18 20)
3	11.63(18 20)	1.00(1 2)	0.361(7 7)	0.0319(6 8)	0.0034(0 3)	13.03(19 20)
4	11.73(19 20)	0.57(1 1)	0.123(3 2)	0.0049(1 1)	$2.3(0 2) \times 10^{-4}$	12.43(19 20)

Table 11. Results for the experimental moments for the maximal selection of data sets. Conventions are as in Tab. 9. All moments are given in units of $10^{-(n+1)} \text{ GeV}^{-2n}$.

are accounted for.

$$C_{\text{uc}}^{\text{exp}} = \begin{pmatrix} 0.04 & 0.034 & 0.033 & 0.034 \\ 0.034 & 0.033 & 0.034 & 0.034 \\ 0.033 & 0.034 & 0.034 & 0.036 \\ 0.034 & 0.034 & 0.036 & 0.037 \end{pmatrix}. \quad (3.22)$$

These results can be used to carry out combined simultaneous fits to several of the moments. This is, however, not attempted in this work.

n	This work	Kuhn et al.'07 [40]	Kuhn et al.'01 [5]	Hoang & Jamin'04 [38]
1	21.21(20 30)	21.66(31)	20.65(84)	20.77(47 90)
2	14.78(18 21)	14.97(27)	14.12(80)	14.05(40 65)
3	13.02(18 20)	13.12(27)	12.34(79)	12.20(41 57)
4	12.43(19 20)	12.49(27)	11.75(79)	11.58(43 53)

Table 12. Comparison of our results for experimental moments to those from previous publications with a dedicated data analysis. The second column contains our results using the default setting. The third and fourth columns were determined from the same collaboration and use data from Refs. [21, 23] (our datasets 2, 4) and [21] (our dataset 2), respectively. The results in the fourth column were also used in the charm mass analysis of Ref. [13]. The numbers in the fifth column used data from Refs. [21, 28, 32] (our datasets 2, 10, 14). The moments in the third column use (slightly less precise) experimental data on the narrow resonances from [81]. The moments in the last two columns were obtained using (less precise) experimental data on the narrow resonances [41]. These data have been updated later [65]. All moments are given in units of $10^{-(n+1)} \text{ GeV}^{-2n}$.

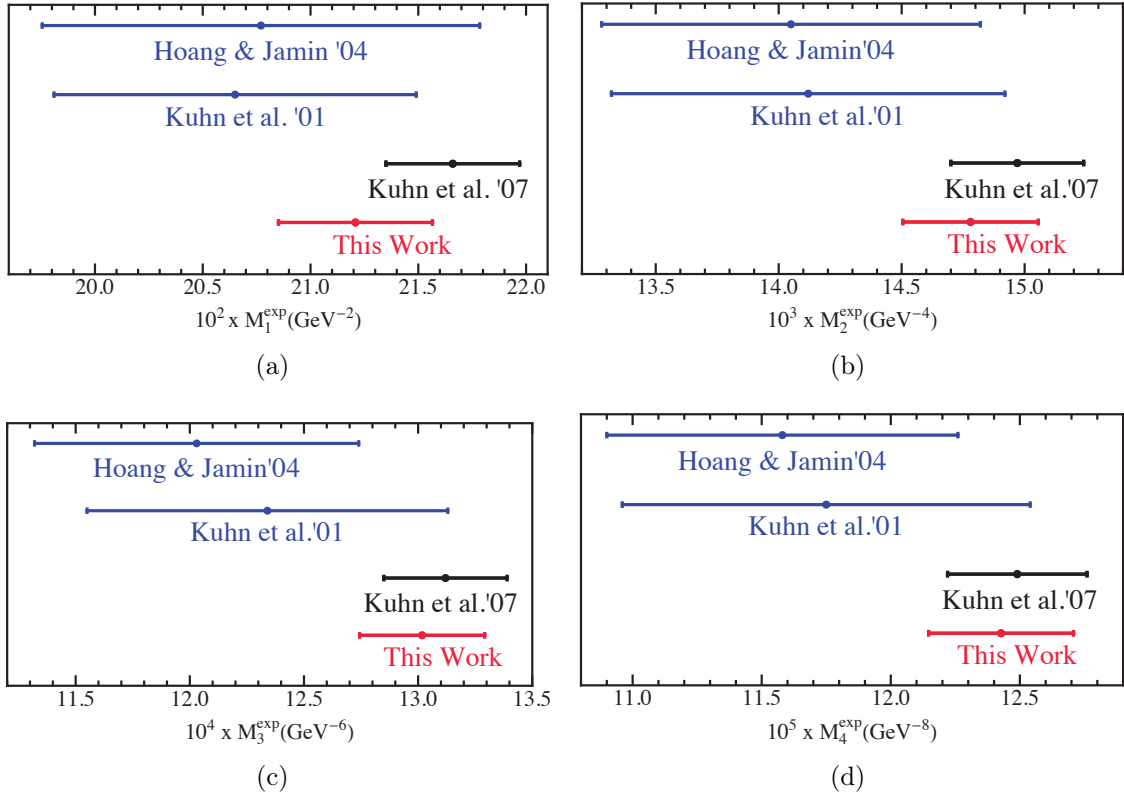


Figure 11. Comparison of determinations of the experimental moments. Blue lines refer to analyses in which outdated values for the parameters of the narrow resonances [41] have been used.

3.4 Examination

We conclude this section with an examination of some of the choices and assumptions we have implemented for the treatment of the experimental uncertainties. Our default choices include

- (i) treating one (quadratic) half of J/ψ and $\psi' e^+e^-$ partial width uncertainties as uncorrelated and the other half as positively correlated among themselves; assuming no correlations of the J/ψ and ψ' partial widths to the R_m cluster values;
- (ii) treating the entire systematical uncertainties of the R -ratio measurements as correlated for the data sets where only total systematical uncertainties were quoted;
- (iii) defining the cluster energies E_m through the weighed average of measurement energies falling into the clusters, see Eq. (3.6);
- (iv) using $N_{cl} = 52 + 1$ clusters distributed in groups of (2,20,20,10) clusters in the energy ranges bounded by (3.73, 3.75, 3.79, 4.55, 10.538) GeV (see Sec. 3.2) and
- (v) using the default data set collection consisting of all data sets discussed in Sec. 3.1 except for sets 16, 17 and 19 as defined in Tab. 7.

In Tab. 13 alternative correlation models are being studied. The second column shows, as a reference, the first four moments with our default settings and the other columns display the results applying changes to the default settings as explained below. The third column displays the moments treating the uncertainties of the J/ψ and ψ' partial widths as uncorrelated. This decreases the total experimental error in $M_{1,2,3,4}^{\text{exp}}$ by (6, 7, 5, 2)%. The fourth column displays the moments treating the uncertainties of the J/ψ and ψ' partial widths being minimally correlated with the R_m values.²¹ Compared to the default setting this increases the total experimental error in $M_{1,2,3,4}^{\text{exp}}$ by (14, 6, 3, 3)%. In the fifth column we display the moments treating, for data sets 1, 6, 13, 15, 16 and 17, one (quadratic) half of systematical uncertainties for the R -values uncorrelated and the other half correlated. In the sixth column all R_m values of all data sets are treated as completely uncorrelated. We see that the central values depend only weakly on the correlation model for those data were the corresponding information is unknown. In particular, for the determination of the uncertainties the ignorance about the composition of the systematical uncertainties in the R -values from data sets 1, 6, 13, 15, 16 and 17 is not essential. However, for quoting the final uncertainties it is important to account for all (known) correlations since they can affect the outcome significantly.

In Tab. 14 we examine the impact of modifying the definition of the cluster energy E_m and of changes to the default cluster distribution (2,20,20,10). In the second column we display the resulting moments of the default setting. In the third and fourth columns we

²¹We use a modified version of the minimal correlation model. The non-diagonal entries of the correlation matrix are filled in with $\Gamma_i R_m \text{Min}^2 \{ \Delta\Gamma_i/\Gamma_i, \Delta R_m/R_m \}$. Here $\Delta\Gamma_i$ and ΔR_m represent the systematical uncertainties of the width of the narrow resonance and the R value of the m -th cluster, respectively, and $i = 1, 2$ refer to J/ψ and ψ' .

n	Default	J/ψ and ψ' uncorr.	Min. overlap to cont.	50% correlation	Uncorrelated
1	21.21(20 30)	21.21(26 22)	21.21(20 36)	21.08(22 31)	20.93(28 24)
2	14.78(18 21)	14.78(25 06)	14.78(18 23)	14.76(19 21)	14.72(20 20)
3	13.02(19 20)	13.02(26 02)	13.02(19 21)	13.02(19 20)	13.02(19 20)
4	12.43(19 20)	12.43(27 01)	12.43(19 20)	12.44(19 20)	12.44(19 20)

Table 13. Dependence on the correlation model. In the second column we show again the results for our default set up. In third column we treat the width of the narrow resonances as uncorrelated. In the fourth column we depict the moments when treating the widths of the narrow resonances as minimally correlated to the values of R_m . In the fifth column we treat the quadratic half of the systematical errors of data sets 1, 6, 13, 15, 16 and 17 as correlated. In the sixth column we show the results when all systematical errors of all data sets are treated as uncorrelated. (Note that in the latter case there is still correlation coming from the narrow resonances and the contributions from the perturbative QCD region). All moments are given in units of $10^{-(n+1)} \text{ GeV}^{-2n}$.

n	Default	Regular average	Middle point	(2, 20, 40, 10)	(2, 10, 20, 10)	(2, 20, 20, 20)
1	21.21(20 30)	21.21(20 30)	21.24(20 29)	21.20(20 30)	21.22(20 30)	21.22(20 29)
2	14.78(18 21)	14.78(18 21)	14.80(18 21)	14.78(18 21)	14.78(18 21)	14.79(18 21)
3	13.02(19 20)	13.02(19 20)	13.03(19 20)	13.02(19 20)	13.02(19 20)	13.02(19 20)
4	12.43(19 20)	12.43(19 20)	12.43(19 20)	12.43(19 20)	12.43(19 20)	12.43(19 20)

Table 14. Stability with clustering. In the second column we show the results for our default set up. In third and fourth column we depict the resulting moments when for the cluster energy we pick the regular average of the energies and the center of the cluster, respectively. In the last three columns we change the default clustering to (2, 20, 40, 10), (2, 10, 20, 10) and (2, 20, 20, 20). All moments are given in units of $10^{-(n+1)} \text{ GeV}^{-2n}$.

have shown the moments using for E_m simply the mean of the energies and the center of the cluster, respectively. The resulting differences to the default definition is an order of magnitude smaller than the uncertainties and thus negligible. The fifth, sixth and seventh columns display the moments using some alternative cluster distributions. The deviations for the default choice illustrated in the table are much smaller than the uncertainties and typical for all modifications that satisfy the guidelines for viable cluster definitions we have formulated in Sec. 3.2. This demonstrates that the choice of the cluster distribution does not result in a bias for the resulting experimental moments.

Finally, we also examine the dependence of the moments on the data set collections as described in Sec. 3.1. In Tabs. 10 and 11 the results for the moments are displayed using the minimal and the maximal collections (with default choices for all other settings). We see that the differences in the central values to the default collection are the same size as the systematical correlated uncertainties for the first moment M_1^{exp} . For the higher moments the differences are much smaller than the uncertainties. Using, instead of the default, the minimal and maximal collections affects the systematic (statistic) uncertainty of M_1^{exp} by only about 10% (5%). For the higher moments the differences decrease strongly and

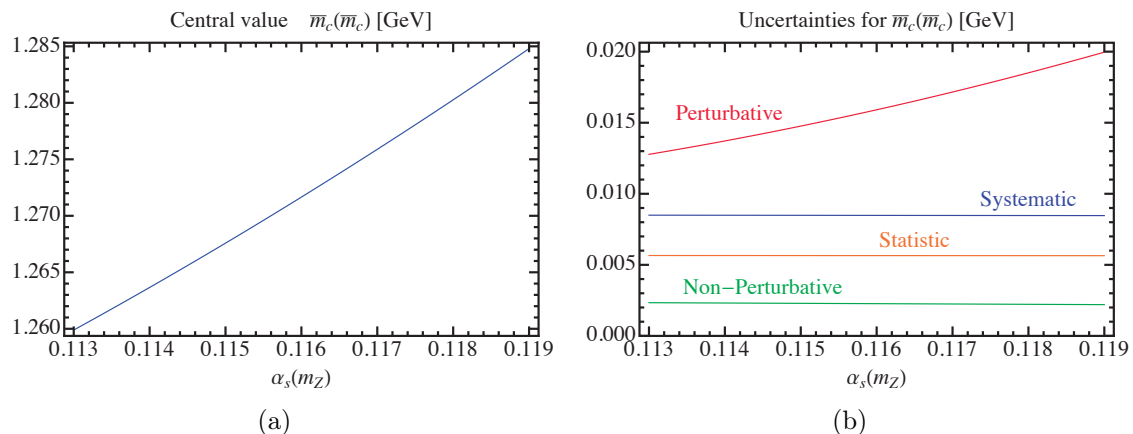


Figure 12. Dependence on $\alpha_s(m_Z)$ of the central values of $\bar{m}_c(\bar{m}_c)$ (a) and its perturbative (b), experimental statistical (c) and experimental systematical (d) errors. The red dots correspond to the values we actually calculated. The blue curve shows an interpolation and the red line in (a) and (b) corresponds to a linear fit.

basically disappear for the fourth moment. Again, the results show that having a slightly increased or decreased redundancy in the data set collection only has a minor impact on the final numbers for the experimental moments.

To summarize, we find that modifications to the choices and assumptions that go into the combined treatment of the experimental data from different publications and experiments lead to changes that are well within the experimental uncertainties we obtain from our combination method. We therefore consider these uncertainties as appropriate. An instructive comparison of the moments obtained in our analysis to those obtained in some previous publications is given in Tab. 12. A graphical illustration of the results is shown in Fig. 11.

4 Charm Quark Mass Analysis for the First Moment

Since it is theoretically most reliable, we use the first moment M_1 as our default for our final numerical charm quark mass analysis. As ingredients for the analysis we use

- (1) the iterative expansion method for the perturbative contribution of the theoretical moment at $\mathcal{O}(\alpha_s^3)$, see Eq. (2.8),
- (2) the gluon condensate correction with its Wilson coefficient determined at $\mathcal{O}(\alpha_s)$ as described in Sec. 2.2,
- (3) the first experimental moment

$$M_1^{\text{exp}} = 0.2121 \pm 0.0020_{\text{stat}} \pm 0.0030_{\text{syst}} \text{ GeV}^{-2}, \quad (4.1)$$

using our default settings as discussed in Sec. 3.

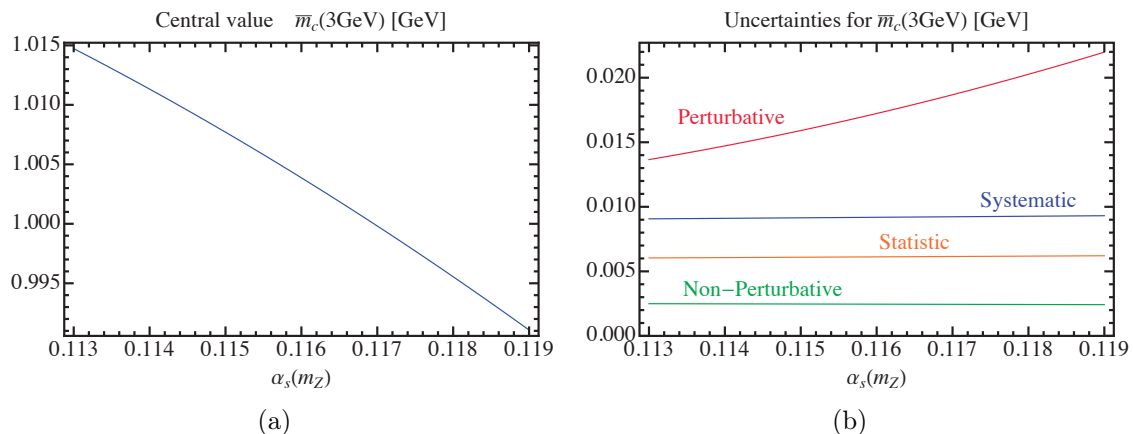


Figure 13. Dependence on $\alpha_s(m_Z)$ of the central values of $\bar{m}_c(3 \text{ GeV})$ (a) and its perturbative (b), experimental statistical (c) and experimental systematical (d) errors. The red dots correspond to the values we actually calculated. The blue curve shows an interpolation and the red line in (a) and (b) corresponds to a linear fit.

$\alpha_s(m_Z)$	$\bar{m}_c(\bar{m}_c)$	Δ_{pert}	Δ_{stat}	Δ_{syst}	$\bar{m}_c(3 \text{ GeV})$	Δ_{pert}	Δ_{stat}	Δ_{syst}
0.113	1.260	0.013	0.006	0.009	1.015	0.014	0.006	0.009
0.114	1.264	0.014	0.006	0.008	1.011	0.015	0.006	0.009
0.115	1.268	0.015	0.006	0.009	1.008	0.016	0.006	0.009
0.116	1.272	0.016	0.006	0.008	1.004	0.017	0.006	0.009
0.117	1.276	0.017	0.006	0.009	1.000	0.019	0.006	0.009
0.118	1.280	0.018	0.006	0.009	0.996	0.020	0.006	0.009
0.119	1.285	0.020	0.006	0.008	0.991	0.022	0.006	0.009

Table 15. Results for the central values of $\bar{m}_c(\bar{m}_c)$ and $\bar{m}_c(3 \text{ GeV})$ (second and sixth columns) and their perturbative (third and seventh columns), experimental statistical (fourth and eighth columns) and experimental systematical (fifth and ninth columns) errors.

One important source of uncertainty we have not yet discussed is the value of the strong $\overline{\text{MS}}$ coupling α_s . Since in the recent literature [82–88] α_s determinations with a spread larger than the current world average [89] have been obtained, we carry out our numerical analysis for values of $\alpha_s(m_Z)$ between 0.113 and 0.119.²² The outcome of our analysis is shown in Tab. 15. In Figs. 12 and 13 the central values, perturbative, statistical and systematical uncertainties are displayed graphically. For the central value and the perturbative uncertainty, which show a significant dependence on α_s , we can present a linear fit. For the statistical and systematical uncertainties the variation with α_s is smaller than 1 MeV and

²² As our default we use $\alpha_s^{n_f=5}(m_Z)$ as the input, use the four-loop QCD beta-function for the renormalization group evolution and three-loop matching conditions to the $n_f = 4$ theory at $\mu = 4.2 \text{ GeV}$.

we only quote constant values. We thus obtain

$$\begin{aligned} \overline{m}_c(\overline{m}_c) &= (1.282 + 4.15 [\alpha_s(m_Z) - 0.1184]) \pm (0.006)_{\text{stat}} \pm (0.009)_{\text{syst}} \\ &\quad \pm (0.019 + 1.20 [\alpha_s(m_Z) - 0.1184])_{\text{pert}} \pm (0.002)_{\langle GG \rangle} \text{ GeV} , \end{aligned} \quad (4.2)$$

$$\begin{aligned} \overline{m}_c(3 \text{ GeV}) &= (0.994 - 3.94 [\alpha_s(m_Z) - 0.1184]) \pm (0.006)_{\text{stat}} \pm (0.009)_{\text{syst}} \\ &\quad \pm (0.021 + 1.39 [\alpha_s(m_Z) - 0.1184])_{\text{pert}} \pm (0.002)_{\langle GG \rangle} \text{ GeV} . \end{aligned} \quad (4.3)$$

Taking as an input

$$\alpha_s(m_Z) = 0.1184 \pm 0.0021 , \quad (4.4)$$

which is the current world Bethke average [89] with a tripled uncertainty we obtain

$$\begin{aligned} \overline{m}_c(\overline{m}_c) &= 1.282 \pm (0.006)_{\text{stat}} \pm (0.009)_{\text{syst}} \pm (0.019)_{\text{pert}} \pm (0.010)_{\alpha_s} \\ &\quad \pm (0.002)_{\langle GG \rangle} \text{ GeV} , \end{aligned} \quad (4.5)$$

$$\begin{aligned} \overline{m}_c(3 \text{ GeV}) &= 0.994 \pm (0.006)_{\text{stat}} \pm (0.009)_{\text{syst}} \pm (0.021)_{\text{pert}} \pm (0.010)_{\alpha_s} \\ &\quad \pm (0.002)_{\langle GG \rangle} \text{ GeV} , \end{aligned} \quad (4.6)$$

which represents, together with Eq. (4.2), our final numerical result for the $\overline{\text{MS}}$ charm mass. Our result is in good agreement with other recent determinations of $\overline{m}_c(\overline{m}_c)$. A summary of the numerical results is shown in Tab. 16 and in Fig. 14. Compared to the analysis carried out in Refs. [39, 40] our experimental uncertainty is larger by 2 MeV and our perturbative uncertainty is larger by 17 MeV, which is a factor of 10 larger. Compared to Refs. [12, 13] the discrepancy in the perturbative error estimate is even larger. Among the most recent high-precision determination of the charm mass based on $\mathcal{O}(\alpha_s^3)$ input from perturbative QCD, our analysis has the biggest error mainly due to our more appropriate treatment of perturbative uncertainties.

5 Higher Moment Analysis

To cross check the results for the charm mass obtained from the first moment M_1 we now carry out an analysis of the moments M_n for $n = 2, 3, 4$ using again the iterative expansion method of the theoretical $\mathcal{O}(\alpha_s^3)$ moments (see Eq. (2.8)) and the gluon condensate correction as discussed in Sec. 2.2. To obtain the perturbative error we again vary the renormalization scales μ_m and μ_α as discussed in Sec. 2.4. The experimental moments are

$$\begin{aligned} M_2^{\text{exp}} &= 0.01478 \pm 0.00018_{\text{stat}} \pm 0.00021_{\text{syst}} \text{ GeV}^{-4} , \\ M_3^{\text{exp}} &= 0.001302 \pm 0.000019_{\text{stat}} \pm 0.000020_{\text{syst}} \text{ GeV}^{-6} , \\ M_4^{\text{exp}} &= 0.0001243 \pm 0.0000019_{\text{stat}} \pm 0.0000020_{\text{syst}} \text{ GeV}^{-8} , \end{aligned} \quad (5.1)$$

using our default settings as discussed in Sec. 3. Due to the strong correlation of the experimental moments there is essentially no gain in statistical power from a combined fit. We therefore carry out individual fits of the higher moments and consider the results

	$\overline{m}_c(\overline{m}_c)$	$\alpha_s(m_Z)$ used	$\overline{m}_c(\overline{m}_c)^{\alpha_s(m_Z)=0.1180}$
This work	1.282 ± 0.024	0.1184 ± 0.0021	1.280 ± 0.023
Chetyrkin et al. [39]	1.279 ± 0.013	0.1189 ± 0.0020	1.277 ± 0.012
Boughezal et al. [13]	1.295 ± 0.015	0.1182 ± 0.0027	–
Hoang & Jamin [38]	1.29 ± 0.07	0.1180 ± 0.0030	1.29 ± 0.07
Bodenstein et al. [67]	1.319 ± 0.026	0.1213 ± 0.0014	1.295 ± 0.026
Bodenstein et al. [44]	1.278 ± 0.009	0.1184 ± 0.0007	–
Narison [68]	1.261 ± 0.018	0.1191 ± 0.0027	–
Allison et al. [42]	1.268 ± 0.009	0.1174 ± 0.0012	–
McNeile et al. [43]	1.273 ± 0.006	0.1183 ± 0.0007	–

Table 16. Comparison of recent determinations of $\overline{m}_c(\overline{m}_c)$. In the second column we show the final result as quoted in the publications, and in the third the value of $\alpha_s(m_Z)$ used in the analysis. In the fourth column, when possible, we extrapolate the results to $\alpha_s(m_Z) = 0.1180$. For the result of Ref. [67] we perform a linear extrapolation using the two values for $\alpha_s(m_Z) = 0.1189$ and 0.1213 quoted in the paper. The last two rows correspond to lattice studies. In the analysis of McNeile et al. the value of $\alpha_s(m_Z)$ was simultaneously determined from the analyses. There have been recent determinations of the charm mass using DIS data, see Refs. [90, 91], which are not included on this table. The values found are in agreement with our determination, but with significantly larger errors. updated table

n	$\overline{m}_c(\overline{m}_c)$	Δ_{stat}	Δ_{syst}	Δ_{pert}	Δ_{α_s}	$\Delta_{\langle GG \rangle}$	Δ_{tot}
1	1.282	0.006	0.009	0.019	0.010	0.002	0.024
2	1.276	0.004	0.004	0.018	0.007	0.004	0.020
3	1.277	0.003	0.003	0.016	0.005	0.004	0.018
4	1.280	0.002	0.002	0.016	0.004	0.005	0.018

Table 17. Results for $\overline{m}_c(\overline{m}_c)$ for the first four moments in GeV units. The first column labels the moment, the central value is shown in the second, statistical and systematical experimental uncertainties are listed in third and fourth column, and the last two columns show errors due to uncertainties in α_s and the gluon condensate. In this table we use the value $\alpha_s(m_Z) = 0.1184 \pm 0.0021$.

as consistency checks of our first moment analysis, and we do not intend to average the results. The results for $\overline{m}_c(\overline{m}_c)$ and $\overline{m}_c(3 \text{ GeV})$ keeping $\alpha_s(m_Z)$ as a parameter are given in App. C. Taking Eq. (4.4) as input for $\alpha_s(m_Z)$ we obtain the results shown in Tab. 17. The results are in excellent agreement with the outcome of the first moment analysis. A graphical comparison of the results with all uncertainties added in quadrature is given in Fig. 15.

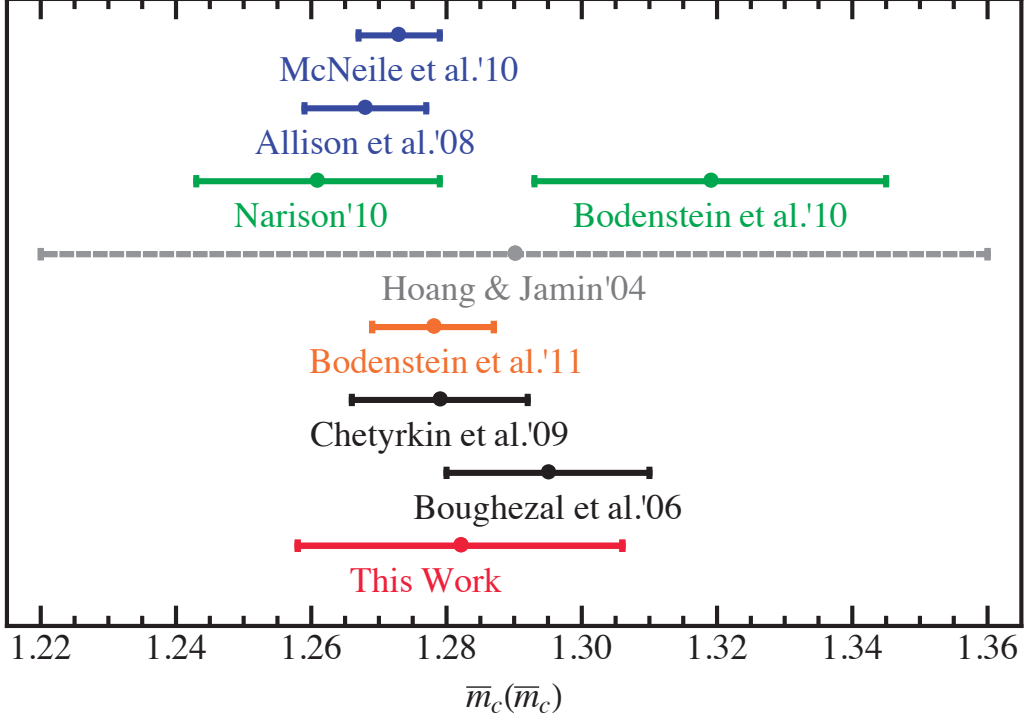


Figure 14. Comparison of recent determinations of $\bar{m}_c(\bar{m}_c)$. Red corresponds to our result, black and gray correspond to $\mathcal{O}(\alpha_s^3)$ and $\mathcal{O}(\alpha_s^2)$ charmonium sum rules analyses, respectively, green labels other kind of sum rule analyses (weighted finite energy sum rules [67] and ratios of Q^2 -dependent moments [68]), and blue stands for lattice simulations.

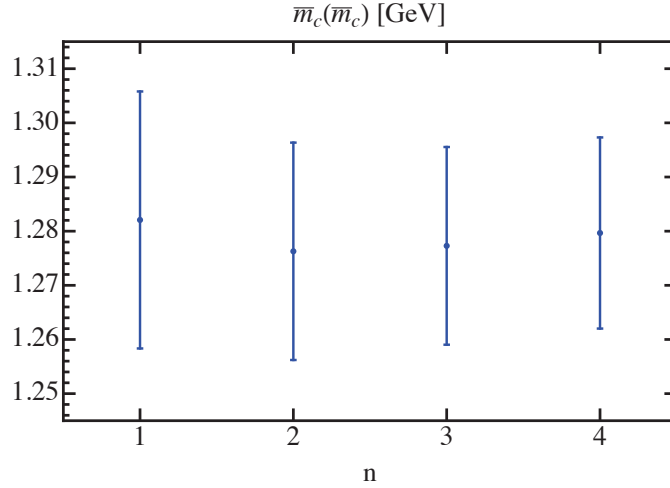


Figure 15. Determination of $\bar{m}_c(\bar{m}_c)$ from the first four moments. We use the expanded out iterative method, including the gluon condensate contribution. All uncertainties have been added in quadrature to compute the shown error bar.

6 Conclusions and Final Thoughts

In this work we have used state-of-the-art $\mathcal{O}(\alpha_s^3)$ input from perturbative QCD to determine the $\overline{\text{MS}}$ charm quark mass from relativistic (low n) charmonium sum rules using experimental data on the total hadronic cross section in e^+e^- annihilation. The main aims were (i) to carefully reexamine perturbative uncertainties in the charm mass extractions from the moments of the charm vector current correlator and (ii) to fully exploit the available experimental data on the hadronic cross section.

We carried out this work having in mind recent $\mathcal{O}(\alpha_s^3)$ sum rule analyses [12, 13, 39, 40, 44], where perturbative errors of 2 MeV or smaller were quoted. Moreover in Refs. [39, 40] an experimental uncertainty of 9 MeV was quoted. Given these numbers we found it appropriate to reexamine this sum rules analysis. In their work the perturbative uncertainty estimate was achieved using a specific choice to arrange the perturbative expansion and by setting the renormalization scales in α_s (μ_α) and of the $\overline{\text{MS}}$ charm quark mass (μ_m) equal. We found that this results in an accidental cancellation of μ_α and μ_m scale variations that is not observed in other alternative ways to treat the perturbative expansion. Moreover, concerning the experimental input their work relied on perturbative QCD predictions instead of available data for energies \sqrt{s} between 4.8 GeV and 10.538 GeV which results in a dependence on the ad-hoc assumption concerning the experimental uncertainty in particular for the first moment.

Concerning the assessment of perturbative and experimental uncertainties we implemented in our work the following improvements:

1. We demonstrated that for achieving an estimate of perturbative uncertainties based on scale variations that is independent of the perturbative expansion method one needs to vary μ_α and μ_m independently, albeit with ranges that avoid large logs. As a result the perturbative uncertainty estimates using different ways to carry out the expansion in α_s become equivalent, which is not the case for $\mu_\alpha = \mu_m$. Another important ingredient of our perturbative error estimate is that we allow renormalization scales at the charm mass $\overline{m}_c(\overline{m}_c)$, where the perturbative expansion is stable, but which was excluded in some of the previous analyses.
2. Using a data clustering method similar to Refs. [46–48] we combined available data on the total e^+e^- hadronic cross section from many different experiments covering energies up to $\sqrt{s} = 10.538$ GeV to fully exploit the existing experimental information for the experimental moments. This avoids a significant dependence of the experimental moments on ad-hoc assumptions on the “experimental” uncertainty being associated to the QCD theory input used for energies above 10.538 GeV. This is because energies above 10.538 GeV only have very small contributions to the low- n moments. As a result we were also able to quantify the correlation between different experimental moments. We also took the opportunity to include recent PDG updates concerning the data for the ψ' resonance.

Using $\alpha_s(m_Z)$ as an unspecified variable and the theoretically more reliable first moment

M_1 for the fits we have obtained

$$\begin{aligned} \overline{m}_c(\overline{m}_c) &= (1.282 + 4.15 [\alpha_s(m_Z) - 0.1184]) \pm (0.006)_{\text{stat}} \pm (0.009)_{\text{syst}} \\ &\quad \pm (0.019 + 1.20 [\alpha_s(m_Z) - 0.1184])_{\text{pert}} \pm (0.002)_{\langle GG \rangle} \text{ GeV} , \end{aligned} \quad (6.1)$$

$$\begin{aligned} \overline{m}_c(3 \text{ GeV}) &= (0.994 - 3.94 [\alpha_s(m_Z) - 0.1184]) \pm (0.006)_{\text{stat}} \pm (0.009)_{\text{syst}} \\ &\quad \pm (0.021 + 1.39 [\alpha_s(m_Z) - 0.1184])_{\text{pert}} \pm (0.002)_{\langle GG \rangle} \text{ GeV} . \end{aligned} \quad (6.2)$$

for the $\overline{\text{MS}}$ charm mass. At the level of uncertainties obtained in our work excellent convergence of perturbation theory was observed. Adopting $\alpha_s(m_Z) = 0.1184 \pm 0.0021$ we then obtain

$$\begin{aligned} \overline{m}_c(\overline{m}_c) &= 1.282 \pm (0.006)_{\text{stat}} \pm (0.009)_{\text{syst}} \pm (0.019)_{\text{pert}} \pm (0.010)_{\alpha_s} \\ &\quad \pm (0.002)_{\langle GG \rangle} \text{ GeV} , \end{aligned} \quad (6.3)$$

$$\begin{aligned} \overline{m}_c(3 \text{ GeV}) &= 0.994 \pm (0.006)_{\text{stat}} \pm (0.009)_{\text{syst}} \pm (0.021)_{\text{pert}} \pm (0.010)_{\alpha_s} \\ &\quad \pm (0.002)_{\langle GG \rangle} \text{ GeV} . \end{aligned} \quad (6.4)$$

Our perturbative error of 19 MeV is a factor of ten larger, and the experimental uncertainty of 11 MeV is by 2 MeV larger than in the most recent analysis of Ref. [40]. For estimating the perturbative error a range of scale variations between $\overline{m}_c(\overline{m}_c)$ and 4 GeV was employed. Adding all uncertainties quadratically we obtain

$$\begin{aligned} \overline{m}_c(\overline{m}_c) &= 1.282 \pm 0.024 \text{ GeV} , \\ \overline{m}_c(3 \text{ GeV}) &= 0.994 \pm 0.026 \text{ GeV} , \end{aligned} \quad (6.5)$$

giving an uncertainty that is twice the size of the one obtained in Refs. [39, 40]. This difference arises mainly from the more appropriate estimate of perturbative uncertainties we obtained in our work.

As a final thought one might ask which further improvements might be possible in the future. As can be seen from Tab. 9, from the experimental side the biggest improvement could be made from more accurate measurements of the J/ψ and ψ' electronic partial widths. The current relative uncertainties are 2.5% and 1.7%, respectively. Here some improvement might be conceivable with dedicated measurements. On theory side, viewing the uncertainties and the good behavior of the perturbative series, it is not unreasonable to assume that the computation of $\mathcal{O}(\alpha_s^4)$ moments of the vector current correlator might further reduce the perturbative error below the level of 20 MeV. Using the $\overline{\text{MS}}$ scheme for the charm mass the OPE states that the remaining perturbative infrared renormalon ambiguity is of order $\Lambda_{\text{QCD}}^4/\overline{m}_c^3 \sim \mathcal{O}(5\text{-}15 \text{ MeV})$. This expectation has also been confirmed by explicit bubble chain (large- β_0) computations [92] and indicates that a further reduction of the perturbative uncertainty is not excluded.

However, to throw in some words of caution, at the level of the present perturbative uncertainties one should also remind oneself about possible loopholes still left in the charmonium sum rule method. An issue we would like to mention concerns the separation of

charm and non-charm hadronic production rates needed to carry out the charmonium sum rule. On the theory side the issue is conceptually subtle due to the singlet and secondary charm radiation contributions which arise at $\mathcal{O}(\alpha_s^3)$ and $\mathcal{O}(\alpha_s^2)$, respectively. In this work (as well as in Ref. [39]) both contributions have been considered as non-charm although they contain terms belonging to the $c\bar{c}$ final state. This treatment might be justified since the size of the corresponding terms are quite small (see Tab. 8) and since it is the common approach to determine the experimental charm production rate in the continuum region by subtracting theoretical results (or models) for the non-charm rate from the measured total hadronic R -ratio. In our method to determine the experimental moments this subtraction involves a normalization constant multiplying the theoretical non-charm R -ratio that is fitted within our clustering method as well accounting for data below and above the charm threshold. The result (see Eq. (A.2)) reveals a disparity of 4% between the theoretical non-charm R -ratio and the data. Setting, in contrast, the normalization constant to unity results in a shift in the charm mass by -15 MeV.²³ Since this shift is compatible with the overall systematical uncertainty in the experimental data, we have not treated it as an additional source of uncertainty. On the other hand, the size of the shift could also be considered as an inherent conceptual uncertainty related to separating the charm from the non-charm R -ratio, which is based on theory considerations rather than on experimental methods and which apparently cannot be improved simply by higher order perturbative computations. We also refer to Refs. [93, 94] for related conceptual discussions. As an alternative, one might avoid the separation of the charm and the non-charm contributions altogether and use the total hadronic cross section for the charm mass fits. Apart from the shift mentioned above such an approach would, however, also lead to a substantially larger dependence on the uncertainties in α_s . Given these considerations we believe that a substantial reduction of the uncertainties also relies on a resolution of the disparity mentioned above. This might certainly involve more precise measurements in the charm threshold and below-threshold regions, but also some deeper conceptual insight. Until then a substantial reduction of the uncertainties shown in Eq. (6.5) appears hard to achieve without imposing ad-hoc assumptions.

Acknowledgments

This work was supported in part by the European Community’s Marie-Curie Research Networks under contract MRTN-CT-2006-035482 (FLAVIANet), MRTN-CT-2006-035505 (HEPTOOLS) and PITN-GA-2010-264564 (LHCphenOnet), and by the U.S. Department of Energy under the grant FG02-94ER40818. V. Mateu has been partially supported by a DFG “Eigenen Stelle” under contract MA 4882/1-1 and by a Marie Curie Fellowship under contract PIOF-GA-2009-251174. S. Zebarjad thanks the MPI for hospitality while part

²³ The same disparity was found in Ref. [40]. In their analysis the corresponding effect is -5 MeV since experimental data were used in the experimental moments only for energies $\sqrt{s} < 4.8$ MeV. In this approach, however, the moments are strongly dependent on the uncertainty one assigns to the theory input used for $\sqrt{s} > 4.8$ MeV.

of this work was accomplished. S. Zebarjad and V. Mateu are grateful to the MPI guest program for partial support. We thank S. Schutzmeier for confirmation of our numerical $\mathcal{O}(\alpha_s^3)$ fixed-order results. A. Hoang acknowledges discussion with H. Kühn and C. Sturm. V. Mateu acknowledges discussion with J. J. Hernández Rey. We thank D. Nomura and T. Teubner for providing us with the effective electromagnetic constant. We thank the *Erwin Schrödinger International Institute for Mathematical Physics* (ESI Vienna), where a part of this work has been accomplished, for partial support.

Appendix A: Results of the Fit Procedure

In this appendix we present in some more detail the numerical results of our fit procedure. In Tabs. A.1, A.2 and A.3, the results for the cluster energies and the cluster charmed R -values are shown for the standard, minimal and maximal selection of data sets, respectively, using our default setting for the correlations. We use the results for the standard data set selection for our final charm mass analysis. The numbers in the parentheses correspond to the statistical and systematical errors. The correlation matrices for the R -values is available, but cannot be displayed due to lack of space. They can be obtained by the authors on request. For the three data selections, the fit gives the following minimal χ^2 per degree of freedom,

$$\frac{\chi_{\text{standard}}^2}{\text{dof}} = 1.89, \quad \frac{\chi_{\text{minimal}}^2}{\text{dof}} = 1.86, \quad \frac{\chi_{\text{maximal}}^2}{\text{dof}} = 1.81, \quad (\text{A.1})$$

and the following normalization constants for the non-charm background

$$n_{\text{ns}}^{\text{standard}} = 1.039 \pm 0.003_{\text{stat}} \pm 0.012_{\text{syst}}, \quad n_{\text{ns}}^{\text{minimal}} = 1.029 \pm 0.003_{\text{stat}} \pm 0.015_{\text{syst}}, \quad (\text{A.2})$$

$$n_{\text{ns}}^{\text{maximal}} = 1.023 \pm 0.003_{\text{stat}} \pm 0.011_{\text{syst}}.$$

The fit results for the normalization constant n_{ns} is compatible with the corresponding normalization constant $n_- = 1.038$ used in Ref. [40] for the subtraction of the non-charm background for the BES 2001 dataset (our data set 2) but is not compatible with the result for the subtraction constant $n_- = 0.991$ concerning the BES 2006 data set (our dataset 5). Since the minimal χ^2/dof values are not close to unity, one has to conclude that the fit quality is not really very good. This is not at all visible from the agreement of the fit and the data for the total cross section (see Figs. 9) and thus might be related to the disparity between the fits of charm versus non-charm production rates described in Sec. 6.

In Eq. (A.3) we show for the correlation matrices of the first four experimental moments for the minimal and the maximal data set selection. The results for our standard selection are given in Eqs. (3.21) and (3.22). All numbers are related to moments M_n^{exp} normalized to units of $10^{-(n+1)} \text{ GeV}^{-2n}$. We show the results accounting for the full set of correlated and uncorrelated uncertainties and the correlation matrices accounting only for uncorrelated systematical and statistical uncertainties (subscript uc).

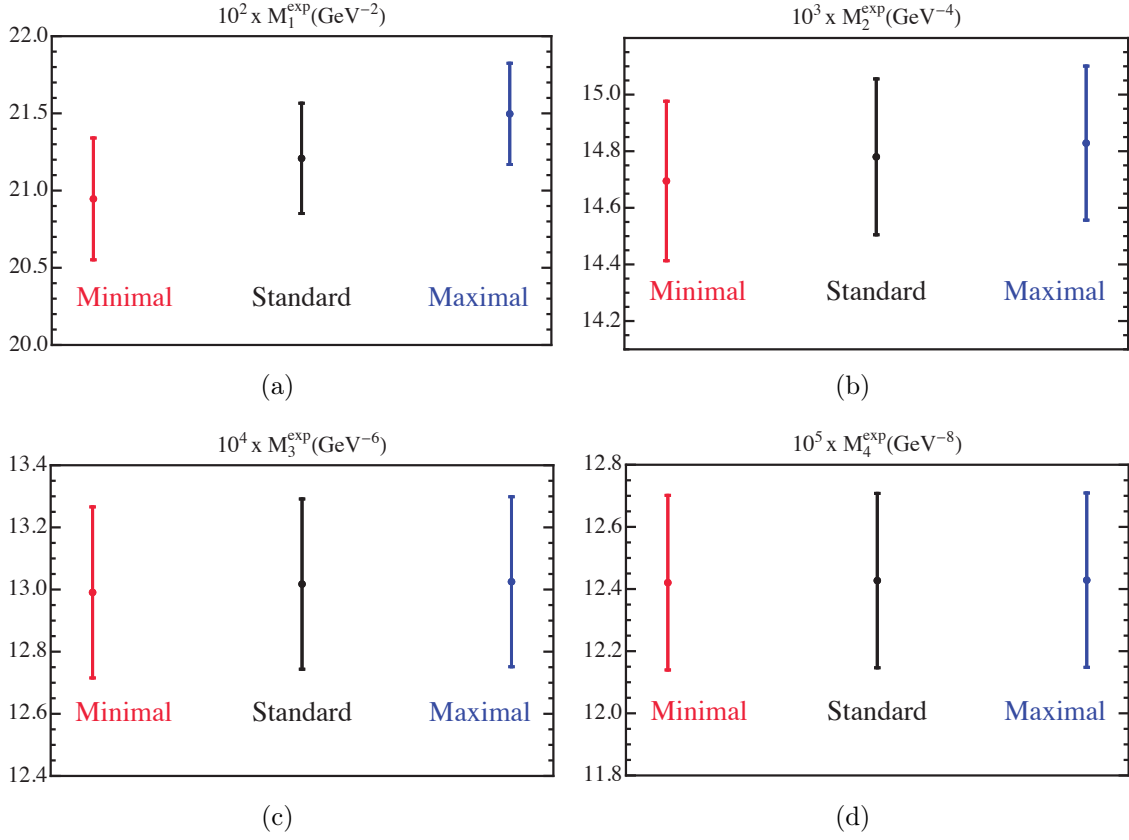


Figure 16. Comparison of the results for the experimental moments using the three data selections.

$$\begin{aligned}
C_{\min}^{\text{exp}} &= \begin{pmatrix} 0.156 & 0.094 & 0.080 & 0.077 \\ 0.094 & 0.079 & 0.076 & 0.076 \\ 0.080 & 0.076 & 0.076 & 0.077 \\ 0.077 & 0.076 & 0.077 & 0.079 \end{pmatrix}, \quad C_{\min, \text{uc}}^{\text{exp}} = \begin{pmatrix} 0.046 & 0.037 & 0.034 & 0.034 \\ 0.037 & 0.034 & 0.034 & 0.035 \\ 0.034 & 0.034 & 0.035 & 0.036 \\ 0.034 & 0.035 & 0.036 & 0.037 \end{pmatrix}, \quad (\text{A.3}) \\
C_{\max}^{\text{exp}} &= \begin{pmatrix} 0.107 & 0.079 & 0.075 & 0.075 \\ 0.079 & 0.074 & 0.074 & 0.075 \\ 0.075 & 0.074 & 0.075 & 0.077 \\ 0.075 & 0.075 & 0.077 & 0.079 \end{pmatrix}, \quad C_{\max, \text{uc}}^{\text{exp}} = \begin{pmatrix} 0.036 & 0.033 & 0.033 & 0.033 \\ 0.033 & 0.033 & 0.033 & 0.034 \\ 0.033 & 0.033 & 0.034 & 0.036 \\ 0.033 & 0.034 & 0.036 & 0.037 \end{pmatrix}.
\end{aligned}$$

Appendix B: On the Equivalence of χ^2 -Functions

In this appendix we demonstrate that a χ^2 -function in which the auxiliary fit parameters d_k , which describe the correlated deviation off the experimental central value within experiment

E	R	E	R	E	R	E	R
3.736	-0.03(6 2)	3.749	0.23(6 2)	3.751	0.47(9 3)	3.753	0.39(7 3)
3.755	0.41(6 3)	3.757	0.80(10 3)	3.759	0.75(7 3)	3.761	0.84(7 3)
3.763	1.06(8 3)	3.765	1.23(9 4)	3.767	1.52(12 4)	3.769	1.31(8 3)
3.771	1.39(6 4)	3.773	1.42(2 4)	3.775	1.22(8 3)	3.777	1.29(8 4)
3.78	1.13(7 3)	3.781	1.06(5 3)	3.783	1.00(7 3)	3.785	0.63(11 3)
3.787	0.64(7 3)	3.79	0.41(5 2)	3.808	0.11(4 2)	3.846	0.10(5 2)
3.883	0.24(7 2)	3.928	0.63(8 2)	3.967	0.94(3 2)	4.002	1.30(3 3)
4.033	2.18(3 4)	4.069	1.74(4 3)	4.117	1.72(4 3)	4.156	1.68(1 4)
4.191	1.54(3 3)	4.23	0.91(5 2)	4.261	0.71(2 2)	4.307	0.89(6 2)
4.346	1.18(6 2)	4.382	1.63(7 3)	4.416	1.76(4 3)	4.452	1.53(7 3)
4.492	1.42(6 3)	4.529	1.29(10 3)	4.715	1.51(3 3)	5.326	1.39(7 7)
6.006	1.33(6 7)	6.596	1.35(7 7)	7.202	1.39(2 4)	7.852	1.52(8 5)
8.417	1.38(3 5)	9.04	1.43(5 6)	9.54	1.35(3 5)	10.327	1.37(1 5)

Table A.1. Best fit values for the standard selection of data sets. The energy of the cluster is measured in GeV, and for R the first number in brackets is the statistical error and the second the systematical one.

E	R	E	R	E	R	E	R
3.736	-0.07(6 2)	3.749	0.22(6 2)	3.751	0.38(9 3)	3.753	0.38(7 3)
3.755	0.40(6 3)	3.757	0.68(11 3)	3.759	0.74(7 3)	3.761	0.82(7 4)
3.763	1.01(8 4)	3.765	1.21(9 4)	3.767	1.49(12 4)	3.769	1.27(8 4)
3.772	1.37(6 4)	3.773	1.38(8 4)	3.775	1.21(8 4)	3.777	1.26(8 4)
3.78	1.11(7 3)	3.781	1.06(5 4)	3.783	0.97(7 4)	3.785	0.62(11 3)
3.787	0.66(8 3)	3.79	0.40(5 3)	3.808	0.11(5 2)	3.845	0.12(5 2)
3.879	0.18(9 2)	3.935	0.85(14 3)	3.969	1.01(4 3)	4.002	1.39(3 4)
4.032	2.25(5 5)	4.066	1.94(4 5)	4.118	1.78(5 5)	4.157	1.77(1 5)
4.191	1.62(3 5)	4.232	0.99(8 3)	4.261	0.76(2 3)	4.309	0.83(10 3)
4.35	1.22(11 3)	4.385	1.28(14 4)	4.415	1.62(10 4)	4.45	1.54(11 4)
4.492	1.30(13 4)	4.529	1.03(13 3)	4.716	1.25(8 3)	5.378	1.40(8 8)
6.008	1.31(7 8)	6.622	1.30(8 8)	7.206	1.37(2 6)	7.856	1.47(8 7)
8.417	1.36(3 6)	9.037	1.40(5 7)	9.544	1.31(3 6)	10.252	1.34(3 6)

Table A.2. Best fit values for the minimal selection of data sets. Conventions are as in Tab. [A.1](#).

E	R	E	R	E	R	E	R
3.736	0.01(6 2)	3.749	0.29(5 2)	3.751	0.48(8 3)	3.753	0.40(7 2)
3.755	0.42(6 3)	3.757	0.80(10 3)	3.759	0.76(7 2)	3.761	0.85(6 3)
3.763	1.06(8 3)	3.765	1.24(8 3)	3.767	1.51(12 4)	3.769	1.31(7 3)
3.771	1.39(6 4)	3.773	1.41(2 4)	3.775	1.21(8 3)	3.777	1.28(8 4)
3.78	1.14(7 3)	3.781	1.06(5 3)	3.783	1.00(7 3)	3.785	0.61(9 3)
3.787	0.64(7 3)	3.79	0.41(5 2)	3.808	0.13(4 2)	3.846	0.10(4 2)
3.884	0.26(5 2)	3.927	0.66(7 2)	3.967	0.98(3 2)	4.002	1.30(2 2)
4.033	2.18(3 3)	4.07	1.74(3 3)	4.117	1.75(4 3)	4.156	1.70(1 4)
4.191	1.54(3 3)	4.23	0.91(5 2)	4.261	0.74(2 2)	4.307	0.87(6 2)
4.346	1.15(5 2)	4.382	1.55(6 3)	4.416	1.80(4 3)	4.452	1.52(6 3)
4.492	1.33(5 2)	4.53	1.19(8 2)	4.722	1.42(3 2)	5.36	1.39(6 4)
6.018	1.47(4 3)	6.608	1.66(4 3)	7.202	1.54(2 3)	7.851	1.63(8 5)
8.417	1.50(3 4)	9.04	1.55(5 5)	9.54	1.47(3 4)	10.327	1.48(1 4)

Table A.3. Best fit values for the maximal selection of data sets. Conventions are as in Tab. A.1.

k , multiplies only the experimental systematical uncertainties,²⁴

$$\chi^2 = \sum_k \left[d_k^2 + \sum_{i,m} \left(\frac{R_i^{k,m} + d_k \Delta_i^{k,m} - R_m}{\sigma_i^{k,m}} \right)^2 \right], \quad (\text{B.1})$$

is mathematically equivalent to the well known χ^2 -function written solely in terms of the fit parameters R_m and a correlation matrix,

$$\bar{\chi}^2 = \sum_{i,j,k,m,n} (R_i^{k,m} - R_m)(V_k^{-1})_{ij}^{mn} (R_j^{k,n} - R_n), \quad (\text{B.2})$$

where there is no correlation among the different experiments k and k' , and the correlation matrix within one experiment k has the form

$$(V_k)_{ij}^{mn} = \sigma_i^{k,m2} \delta_{ij} \delta^{mn} + \Delta_i^{k,m} \Delta_j^{k,n}. \quad (\text{B.3})$$

The matrix Eq. (B.3) can be inverted analytically giving

$$(V_k^{-1})_{ij}^{mn} = \frac{\delta_{ij} \delta^{mn}}{(\sigma_i^{k,m})^2} - \frac{1}{1 + \frac{\langle \Delta^2 \rangle_k}{\langle \sigma \rangle_k^2}} \frac{\Delta_i^{k,m}}{(\sigma_i^{k,m})^2} \frac{\Delta_j^{k,n}}{(\sigma_j^{k,n})^2}, \quad (\text{B.4})$$

²⁴ For the discussion in this appendix we do for simplicity of the presentation not account for fits of the non-charm contribution. It is, however, straightforward to generalize the presentation to this case.

where we have defined the mean statistical error and the statistical average of the systematic error within one experiment as follows:

$$\langle \sigma \rangle_k^2 \equiv \left(\sum_{i,m} \frac{1}{(\sigma_i^{k,m})^2} \right)^{-1}, \quad \langle \Delta^2 \rangle_k \equiv \langle \sigma \rangle_k^2 \sum_{i,m} \frac{(\Delta_i^{k,m})^2}{(\sigma_i^{k,m})^2}. \quad (\text{B.5})$$

In case of a sizable positive correlation between measurements in the same experiment (such that $\Delta_i^{k,m}/R_i^{k,m}$ is sizable and approximately constant) it is known that the form of the χ^2 -function in Eq. (B.1) leads to best fit values R_m that are systematically below the measurements [46]. Our proof demonstrates that the standard χ^2 -function of Eq. (B.2) has the same property for correlation matrices with the form of Eq. (B.3). This motivates to use the so-called minimal-overlap correlation model where the second term on the RHS of Eq. (B.2) is replaced by $\min^2(\Delta_i^{k,m}, \Delta_j^{k,n})$. In general, within the minimal-overlap model, the correlations are sufficiently reduced such that the unphysical effect described above does not arise.

We proceed by showing that one can “integrate out” auxiliary parameters d_k in Eq. (B.1) obtaining a new function $\tilde{\chi}^2(R^i)$ which yields the same results for the best fit for the R_m , as long as one works in the Gaussian approximation. The minimum of $\chi^2(R_i, d_k)$ is located at the best fit values (indicated by superscripts (0)) defined by the conditions

$$\left. \frac{\partial \chi^2}{\partial R_i} \right|_{R_i^{(0)}, d_k^{(0)}} = \left. \frac{\partial \chi^2}{\partial d_j} \right|_{R_i^{(0)}, d_k^{(0)}} = 0. \quad (\text{B.6})$$

To invert the matrix of second derivatives we proceed in blocks

$$\begin{pmatrix} \frac{\partial^2 \chi^2}{\partial R_i \partial R_j} & \frac{\partial^2 \chi^2}{\partial R_i \partial d_k} \\ \frac{\partial^2 \chi^2}{\partial d_l \partial R_j} & \frac{\partial^2 \chi^2}{\partial d_l \partial d_k} \end{pmatrix}_{\tilde{R}, \tilde{b}} \begin{pmatrix} c_{jm} & b_{jr} \\ b_{mk} & a_{kr} \end{pmatrix} = \begin{pmatrix} \delta_{im} & 0 \\ 0 & \delta_{lr} \end{pmatrix}. \quad (\text{B.7})$$

where c_{ij} and a_{kr} are $N_{\text{cluster}} \times N_{\text{cluster}}$ and $N_{\text{exp}} \times N_{\text{exp}}$ square matrices, respectively, and b_{jr} is a $N_{\text{cluster}} \times N_{\text{exp}}$ rectangular matrix. We find the following four matrix relations

$$\sum_j \frac{\partial^2 \chi^2}{\partial R_i \partial R_j} c_{jm} + \sum_k \frac{\partial^2 \chi^2}{\partial R_i \partial d_k} b_{mk} = \delta_{im}, \quad \sum_j \frac{\partial^2 \chi^2}{\partial R_i \partial R_j} b_{jr} + \sum_k \frac{\partial^2 \chi^2}{\partial R_i \partial d_k} a_{kr} = 0, \quad (\text{B.8})$$

$$\sum_j \frac{\partial^2 \chi^2}{\partial d_l \partial R_j} c_{jm} + \sum_k \frac{\partial^2 \chi^2}{\partial d_l \partial d_k} b_{mk} = 0, \quad \sum_j \frac{\partial^2 \chi^2}{\partial d_l \partial R_j} b_{jr} + \sum_k \frac{\partial^2 \chi^2}{\partial d_l \partial d_k} a_{kr} = \delta_{lr}. \quad (\text{B.9})$$

Combining Eqs. (B.8a) and (B.9a) we find the inverse of the upper left R -block,

$$(c^{-1})_{ij} = 2(V^{-1})_{ij} = \frac{\partial^2 \chi^2}{\partial R_i \partial R_j} - \sum_{kl} \frac{\partial^2 \chi^2}{\partial d_l \partial R_i} \left[\frac{\partial^2 \chi^2}{\partial d_l \partial d_k} \right]^{-1} \frac{\partial^2 \chi^2}{\partial d_k \partial R_j}, \quad (\text{B.10})$$

where $\left[\frac{\partial^2 \chi^2}{\partial d_l \partial d_k} \right]^{-1}$ stands for the (l, k) element of the inverse matrix of $\frac{\partial^2 \chi^2}{\partial d_l \partial d_k}$ (and not the inverse of the element). Combining Eqs. (B.8b) and (B.9b) one can obtain relations for

the a and b submatrices:

$$b_{jr} = - \sum_{i,k} \left[\frac{\partial^2 \chi^2}{\partial R_j \partial R_i} \right]^{-1} \frac{\partial^2 \chi^2}{\partial d_k \partial R_i} a_{kr}, \quad (\text{B.11})$$

$$\delta_{lr} = \sum_k \left(\frac{\partial^2 \chi^2}{\partial d_l \partial d_k} - \sum_{i,j} \frac{\partial^2 \chi^2}{\partial d_l \partial R_j} \left[\frac{\partial^2 \chi^2}{\partial R_j \partial R_i} \right]^{-1} \frac{\partial^2 \chi^2}{\partial d_i \partial R_k} \right) a_{kr}, \quad (\text{B.12})$$

$$\delta_{im} = \sum_j \frac{\partial^2 \chi^2}{\partial R_i \partial R_j} c_{jm} - \sum_{k,l,s} \frac{\partial^2 \chi^2}{\partial d_k \partial R_i} \left[\frac{\partial^2 \chi^2}{\partial R_m \partial R_s} \right]^{-1} \frac{\partial^2 \chi^2}{\partial d_l \partial R_s} a_{lk}, \quad (\text{B.13})$$

where again $\left[\frac{\partial^2 \chi^2}{\partial R_j \partial R_i} \right]^{-1}$ stands for the (j, i) element of the inverse matrix of $\frac{\partial^2 \chi^2}{\partial R_j \partial R_i}$. We “integrate out” the auxiliary parameters d_k by substituting their minimum conditions $d_k^{(0)} = \tilde{d}_k(R_i^{(0)})$ (which is analogous to using the equation of motion when integrating out heavy particles):

$$\left. \frac{\partial \chi^2}{\partial d_j} \right|_{d_k = \tilde{d}_k(R_i)} = 0, \quad \tilde{\chi}^2(R_i) = \chi^2(R_i, \tilde{d}_k(R_i)). \quad (\text{B.14})$$

Their first derivatives with respect to R_j read

$$\begin{aligned} \frac{\partial}{\partial R_j} \left. \frac{\partial \chi^2}{\partial d_i} \right|_{\tilde{d}_m(R_k)} &= \left. \frac{\partial^2 \chi^2}{\partial d_i \partial R_j} \right|_{\tilde{d}_m(R_k)} + \sum_l \left. \frac{\partial^2 \chi^2}{\partial d_i \partial d_l} \right|_{\tilde{d}_m(R_k)} \frac{\partial \tilde{d}_l(R_n)}{\partial R_j} = 0, \\ \frac{\partial \tilde{d}_i(R_n)}{\partial R_j} &= - \sum_l \left[\frac{\partial^2 \chi^2}{\partial d_i \partial d_l} \right]_{\tilde{d}_m(R_k)}^{-1} \left. \frac{\partial^2 \chi^2}{\partial d_l \partial R_j} \right|_{\tilde{d}_m(R_k)}. \end{aligned} \quad (\text{B.15})$$

The minimum of $\tilde{\chi}^2(R_i)$ is indeed located at $R_i^{(0)}$ because

$$\frac{\partial \tilde{\chi}^2}{\partial R_i} = \sum_k \left. \frac{\partial \chi^2}{\partial d_k} \right|_{d_k = \tilde{d}_k(R_i)} \frac{d \tilde{d}_k}{d R_i} + \left. \frac{\partial \chi^2}{\partial R_i} \right|_{d_k = \tilde{d}_k(R_i)} = \left. \frac{\partial \chi^2}{\partial R_i} \right|_{d_k = \tilde{d}_k(R_i)}, \quad (\text{B.16})$$

and because the first term vanishes by the condition in Eq. (B.14). When evaluating Eq. (B.16) for $R_i = R_i^{(0)}$ it vanishes because of Eq. (B.6). Finally, let us calculate the inverse correlation matrix:

$$\begin{aligned} \left. \frac{\partial^2 \tilde{\chi}^2}{\partial R_i \partial R_j} \right|_{\tilde{R}_k} &= \left. \frac{\partial^2 \chi^2}{\partial R_i \partial R_j} \right|_{d_m^{(0)}, R_k^{(0)}} + \sum_k \left. \frac{\partial^2 \chi^2}{\partial d_k \partial R_j} \right|_{d_m^{(0)}, R_k^{(0)}} \left. \frac{\partial \tilde{d}_k(R_i)}{\partial R_i} \right|_{\tilde{R}_k} \\ &= \left. \frac{\partial^2 \chi^2}{\partial R_i \partial R_j} \right|_{d^{(0)}, R_k^{(0)}} - \sum_{k,l} \left[\frac{\partial^2 \chi^2}{\partial d_k \partial d_l} \right]_{d_m^{(0)}, R_k^{(0)}}^{-1} \left. \frac{\partial^2 \chi^2}{\partial d_l \partial R_i} \right|_{d_m^{(0)}, R_k^{(0)}} \left. \frac{\partial^2 \chi^2}{\partial d_k \partial R_j} \right|_{d_m^{(0)}, R_k^{(0)}}, \end{aligned} \quad (\text{B.17})$$

which agrees with Eq. (B.10).

We can now apply the previous results to Eq. (B.1):

$$\begin{aligned} \chi^2 &= \sum_k \left[d_k^2 + \sum_{i,m} \left(\frac{R_i^{k,m} + d_k \Delta_i^{k,m} - R_m}{\sigma_i^{k,m}} \right)^2 \right] \\ &= \sum_k \left\{ d_k^2 \left[1 + \frac{\langle \Delta^2 \rangle_k}{\langle \sigma \rangle_k^2} \right] + 2 d_k \sum_{i,m} \frac{(R_i^{k,m} - R_m) \Delta_i^k}{\sigma_i^{k,m} 2} + \sum_{i,m} \left(\frac{R_i^{k,m} - R_m}{\sigma_i^{k,m}} \right)^2 \right\}. \end{aligned} \quad (\text{B.18})$$

The equation of motion for d_k reads

$$d_k(R) = - \frac{1}{1 + \frac{\langle \Delta^2 \rangle_k}{\langle \sigma \rangle_k^2}} \sum_{i,m} \frac{(R_i^{k,m} - R_m) \Delta_i^{k,m}}{\sigma_i^{k,m 2}}. \quad (\text{B.19})$$

This renders for $\tilde{\chi}^2$ the form

$$\begin{aligned} \tilde{\chi}^2 &= \sum_k \left[d_k(R) \sum_{i,m} \frac{(R_i^{k,m} - R_m) \Delta_i^{k,m}}{\sigma_i^{k,m 2}} + \sum_{i,m} \left(\frac{R_i^{k,m} - R_m}{\sigma_i^{k,m}} \right)^2 \right] \\ &= \sum_k \left[\sum_{i,m} \left(\frac{R_i^{k,m} - R_m}{\sigma_i^{k,m}} \right)^2 - \frac{1}{1 + \frac{\langle \Delta^2 \rangle_k}{\langle \sigma \rangle_k^2}} \sum_{i,j,m,n} \frac{(R_i^{k,m} - R_m) \Delta_i^{k,m}}{\sigma_i^{k,m 2}} \frac{(R_j^{k,n} - R_n) \Delta_j^{k,n}}{\sigma_j^{k,n 2}} \right], \end{aligned} \quad (\text{B.20})$$

which reproduces Eq. (B.2), as we wanted to demonstrate.

We conclude this appendix presenting an alternative way to write Eq. (3.11) after using the equations of motion for d_k . We again concentrate on the simpler case without subtraction of the non-charm contribution:

$$\begin{aligned} \chi^2 &= \sum_k \left\{ d_k^2 + \sum_{i,m} \left[\frac{R_i^{k,m} - (1 + d_k \Delta f_k^{i,m}) R_m}{\sigma_k^{i,m}} \right]^2 \right\} \\ &= \sum_k \left\{ \left[1 + \sum_{i,m} \left(\frac{\Delta f_k^{i,m} R_m}{\sigma_k^{i,m}} \right)^2 \right] d_k^2 - 2d_k \sum_{i,m} \frac{(R_k^{i,m} - R_m) \Delta f_k^{i,m} R_m}{(\sigma_k^{i,m})^2} \right. \\ &\quad \left. + \sum_{i,m} \left[\frac{R_k^{i,m} - R_m}{\sigma_k^{i,m}} \right]^2 \right\}. \end{aligned} \quad (\text{B.21})$$

The EOM for d_k now reads

$$\left[1 + \sum_{i,m} \left(\frac{\Delta f_k^{i,m} R_m}{\sigma_k^{i,m}} \right)^2 \right] \tilde{d}_k(R_n) - \sum_{i,m} \frac{(R_k^{i,m} - R_m) \Delta f_k^{i,m} R_m}{(\sigma_k^{i,m})^2} = 0, \quad (\text{B.22})$$

which upon insertion into Eq. (B.21) renders

$$\begin{aligned} \tilde{\chi}^2 &= \sum_k \left\{ \sum_{i,m} \left[\frac{R_k^{i,m} - R_m}{\sigma_k^{i,m}} \right]^2 - \tilde{d}_k(R_n) \sum_{i,m} \frac{(R_k^{i,m} - R_m) \Delta f_k^{i,m} R_m}{(\sigma_k^{i,m})^2} \right\} \\ &= \sum_k \left\{ \sum_{i,m} \left[\frac{R_k^{i,m} - R_m}{\sigma_k^{i,m}} \right]^2 \right. \\ &\quad \left. - \frac{1}{\left[1 + \sum_{i,m} \left(\frac{\Delta f_k^{i,m} R_m}{\sigma_k^{i,m}} \right)^2 \right]} \left[\sum_{i,m} \frac{(R_k^{i,m} - R_m) \Delta f_k^{i,m} R_m}{(\sigma_k^{i,m})^2} \right]^2 \right\}. \end{aligned} \quad (\text{B.23})$$

One can rewrite Eq. (B.23) in the matrix form

$$\begin{aligned}\tilde{\chi}^2 &= \sum_k \left\{ \sum_{i,j,m,n} [R_k^{im} - R_m] [V_k^{-1}]^{mn} [R_k^{jn} - R_n] \right\}, \\ [V_k^{-1}]^{mn} &= \frac{\delta_{ij} \delta^{mn}}{(\sigma_k^{i,m})^2} - \frac{\left(R_k^{i,m} - R_m \right) \Delta f_k^{i,m} R_m \left(R_k^{jn} - R_n \right) \Delta f_k^{jn} R_n}{\left[1 + \sum \left(\frac{\Delta_k^{i,m} R_m}{\sigma_k^{i,m}} \right)^2 \right]}.\end{aligned}\quad (\text{B.24})$$

In Eq. (B.24) one can interpret the second term of the inverse correlation matrix, as a non-linear correlation among the measurements, where the correlation matrix itself depends on the value of the fit parameters. The total inverse correlation matrix is block diagonal, and the blocks correspond to V_k^{-1} .

Appendix C: Dependence on α_s for Higher Moment Analyses

In this appendix we display the dependence of $\overline{m}_c(\overline{m}_c)$ and for $\overline{m}_c(3 \text{ GeV})$ on the value of the strong coupling constant at the Z pole, when fitted from the second, third and fourth moments. These results are the equivalent of Eq. (4.2). The results for the canonical value $\alpha_s(m_Z) = 0.1184 \pm 0.0021$ are shown in Tab. 17.

- $n = 2$

$$\begin{aligned}\overline{m}_c(\overline{m}_c) &= (1.276 + 2.90 [\alpha_s(m_Z) - 0.1184]) \pm (0.004)_{\text{stat}} \pm (0.004)_{\text{syst}} \\ &\quad \pm (0.017 + 1.14 [\alpha_s(m_Z) - 0.1184])_{\text{pert}} \pm (0.004)_{\langle GG \rangle} \text{ GeV},\end{aligned}\quad (\text{C.1})$$

$$\begin{aligned}\overline{m}_c(3 \text{ GeV}) &= (0.988 - 5.32 [\alpha_s(m_Z) - 0.1184]) \pm (0.002)_{\text{stat}} \pm (0.002)_{\text{syst}} \\ &\quad \pm (0.019 + 1.31 [\alpha_s(m_Z) - 0.1184])_{\text{pert}} \pm (0.004)_{\langle GG \rangle} \text{ GeV}.\end{aligned}\quad (\text{C.2})$$

- $n = 3$

$$\begin{aligned}\overline{m}_c(\overline{m}_c) &= (1.277 + 2.12 [\alpha_s(m_Z) - 0.1184]) \pm (0.003)_{\text{stat}} \pm (0.003)_{\text{syst}} \\ &\quad \pm (0.016 + 1.08 [\alpha_s(m_Z) - 0.1184])_{\text{pert}} \pm (0.004)_{\langle GG \rangle} \text{ GeV},\end{aligned}\quad (\text{C.3})$$

$$\begin{aligned}\overline{m}_c(3 \text{ GeV}) &= (0.989 - 6.14 [\alpha_s(m_Z) - 0.1184]) \pm (0.003)_{\text{stat}} \pm (0.003)_{\text{syst}} \\ &\quad \pm (0.018 + 1.25 [\alpha_s(m_Z) - 0.1184])_{\text{pert}} \pm (0.005)_{\langle GG \rangle} \text{ GeV}.\end{aligned}\quad (\text{C.4})$$

- $n = 4$

$$\begin{aligned}\overline{m}_c(\overline{m}_c) &= (1.279 + 1.55 [\alpha_s(m_Z) - 0.1184]) \pm (0.002)_{\text{stat}} \pm (0.002)_{\text{syst}} \\ &\quad \pm (0.016 + 1.05 [\alpha_s(m_Z) - 0.1184])_{\text{pert}} \pm (0.005)_{\langle GG \rangle} \text{ GeV},\end{aligned}\quad (\text{C.5})$$

$$\begin{aligned}\overline{m}_c(3 \text{ GeV}) &= (0.992 - 6.75 [\alpha_s(m_Z) - 0.1184]) \pm (0.003)_{\text{stat}} \pm (0.003)_{\text{syst}} \\ &\quad \pm (0.017 + 1.21 [\alpha_s(m_Z) - 0.1184])_{\text{pert}} \pm (0.006)_{\langle GG \rangle} \text{ GeV}.\end{aligned}\quad (\text{C.6})$$

References

- [1] M. Antonelli et al., *Flavor Physics in the Quark Sector*, *Phys. Rept.* **494** (2010) 197–414, [[arXiv:0907.5386](#)].
- [2] V. A. Novikov et al., *Charmonium and Gluons: Basic Experimental Facts and Theoretical Introduction*, *Phys. Rept.* **41** (1978) 1–133.
- [3] M. A. Shifman, A. I. Vainshtein, and V. I. Zakharov, *QCD and Resonance Physics. Sum Rules*, *Nucl. Phys.* **B147** (1979) 385–447.
- [4] M. A. Shifman, A. I. Vainshtein, and V. I. Zakharov, *QCD and Resonance Physics: Applications*, *Nucl. Phys.* **B147** (1979) 448–518.
- [5] J. H. Kuhn and M. Steinhauser, *Determination of α_s and heavy quark masses from recent measurements of $R(s)$* , *Nucl. Phys.* **B619** (2001) 588–602, [[hep-ph/0109084](#)].
- [6] A. O. G. Kallen and A. Sabry, *Fourth order vacuum polarization*, *Kong. Dan. Vid. Sel. Mat. Fys. Med.* **29N17** (1955) 1–20.
- [7] K. Chetyrkin, J. H. Kuhn, and M. Steinhauser, *Heavy quark vacuum polarization to three loops*, *Phys. Lett.* **B371** (1996) 93–98, [[hep-ph/9511430](#)].
- [8] K. Chetyrkin, J. H. Kuhn, and M. Steinhauser, *Three loop polarization function and $O(\alpha_s^2)$ corrections to the production of heavy quarks*, *Nucl. Phys.* **B482** (1996) 213–240, [[hep-ph/9606230](#)].
- [9] R. Boughezal, M. Czakon, and T. Schutzmeier, *Four-loop tadpoles: Applications in QCD*, *Nucl. Phys. Proc. Suppl.* **160** (2006) 160–164, [[hep-ph/0607141](#)].
- [10] M. Czakon and T. Schutzmeier, *Double fermionic contributions to the heavy-quark vacuum polarization*, *JHEP* **0807** (2008) 001, [[arXiv:0712.2762](#)].
- [11] A. Maier, P. Maierhofer, and P. Marquard, *Higher Moments of Heavy Quark Correlators in the Low Energy Limit at $O(\alpha_s^2)$* , *Nucl. Phys.* **B797** (2008) 218–242, [[arXiv:0711.2636](#)].
- [12] K. G. Chetyrkin, J. H. Kuhn, and C. Sturm, *Four-loop moments of the heavy quark vacuum polarization function in perturbative QCD*, *Eur. Phys. J.* **C48** (2006) 107–110, [[hep-ph/0604234](#)].
- [13] R. Boughezal, M. Czakon, and T. Schutzmeier, *Charm and bottom quark masses from perturbative QCD*, *Phys. Rev.* **D74** (2006) 074006, [[hep-ph/0605023](#)].
- [14] A. Maier, P. Maierhofer, and P. Marquard, *The second physical moment of the heavy quark vector correlator at $O(\alpha_s^3)$* , *Phys. Lett.* **B669** (2008) 88–91, [[arXiv:0806.3405](#)].
- [15] A. Maier, P. Maierhofer, P. Marquard, and A. V. Smirnov, *Low energy moments of heavy quark current correlators at four loops*, *Nucl. Phys.* **B824** (2010) 1–18, [[arXiv:0907.2117](#)].
- [16] A. H. Hoang, V. Mateu, and S. Mohammad Zabarjad, *Heavy Quark Vacuum Polarization Function at $O(\alpha_s^2)$ and $O(\alpha_s^3)$* , *Nucl. Phys.* **B813** (2009) 349–369, [[arXiv:0807.4173](#)].
- [17] Y. Kiyo, A. Maier, P. Maierhofer, and P. Marquard, *Reconstruction of heavy quark current correlators at $O(\alpha_s^3)$* , *Nucl. Phys.* **B823** (2009) 269–287, [[arXiv:0907.2120](#)].
- [18] D. Greynat and S. Peris, *Resummation of Threshold, Low- and High-Energy Expansions for Heavy-Quark Correlators*, *Phys. Rev.* **D82** (2010) 034030, [[arXiv:1006.0643](#)].

- [19] D. J. Broadhurst et al., *Two loop gluon condensate contributions to heavy quark current correlators: Exact results and approximations*, *Phys. Lett.* **B329** (1994) 103–110, [[hep-ph/9403274](#)].
- [20] **BES** Collaboration, J. Z. Bai et al., *Measurement of the Total Cross Section for Hadronic Production by e^+e^- Annihilation at Energies between 2.6 – 5 GeV*, *Phys. Rev. Lett.* **84** (2000) 594–597, [[hep-ex/9908046](#)].
- [21] **BES** Collaboration, J. Z. Bai et al., *Measurements of the Cross Section for $e^+e^- \rightarrow$ hadrons at Center-of-Mass Energies from 2 to 5 GeV*, *Phys. Rev. Lett.* **88** (2002) 101802, [[hep-ex/0102003](#)].
- [22] **BES** Collaboration, M. Ablikim et al., *Measurement of Cross Sections for $D^0\bar{D}^0$ and D^+D^- Production in e^+e^- Annihilation at $\sqrt{s} = 3.773$ GeV*, *Phys. Lett.* **B603** (2004) 130–137, [[hep-ex/0411013](#)].
- [23] **BES** Collaboration, M. Ablikim et al., *Measurements of the cross sections for $e^+e^- \rightarrow$ hadrons at 3.650 GeV, 3.6648 GeV, 3.773 GeV and the branching fraction for $\psi(3770) \rightarrow$ non $D\bar{D}$* , *Phys. Lett.* **B641** (2006) 145–155, [[hep-ex/0605105](#)].
- [24] M. Ablikim et al., *Measurements of the continuum R_{uds} and R values in e^+e^- annihilation in the energy region between 3.650 GeV and 3.872 GeV*, *Phys. Rev. Lett.* **97** (2006) 262001, [[hep-ex/0612054](#)].
- [25] **BES Collaboration**, M. Ablikim et al., *R value measurements for e^+e^- annihilation at 2.60, 3.07 and 3.65 GeV*, *Phys. Lett.* **B677** (2009) 239–245, [[arXiv:0903.0900](#)].
- [26] Osterheld et al., *Measurements of total hadronic and inclusive D^* cross-sections in e^+e^- annihilations between 3.87 GeV and 4.5 GeV*, *Phys. Rev. D* (1986).
- [27] C. Edwards et al., *Hadron production in e^+e^- annihilation from $s^{1/2} = 5$ GeV to 7.4 GeV*, . SLAC-PUB-5160.
- [28] **CLEO** Collaboration, R. Ammar et al., *Measurement of the total cross section for $e^+e^- \rightarrow$ hadrons at $s^{1/2} = 10.52$ GeV*, *Phys. Rev.* **D57** (1998) 1350–1358, [[hep-ex/9707018](#)].
- [29] **CLEO** Collaboration, D. Besson et al., *Observation of New Structure in the e^+e^- Annihilation Cross-Section Above $B\bar{B}$ Threshold*, *Phys. Rev. Lett.* **54** (1985) 381.
- [30] **CLEO** Collaboration, D. Besson et al., *Measurement of the Total Hadronic Cross Section in e^+e^- Annihilations below 10.56 GeV*, *Phys. Rev.* **D76** (2007) 072008, [[arXiv:0706.2813](#)].
- [31] **CLEO** Collaboration, D. Cronin-Hennessy et al., *Measurement of Charm Production Cross Sections in e^+e^- Annihilation at Energies between 3.97 and 4.26 GeV*, *Phys. Rev.* **D80** (2009) 072001, [[arXiv:0801.3418](#)].
- [32] A. E. Blinov et al., *The Measurement of R in e^+e^- annihilation at center-of-mass energies between 7.2 GeV and 10.34 GeV*, *Z. Phys.* **C70** (1996) 31–38.
- [33] L. Criegee and G. Knies, *Review of e^+e^- experiments with PLUTO from 3 GeV to 31 GeV*, *Phys. Rept.* **83** (1982) 151.
- [34] J. Siegrist et al., *Observation of a Resonance at 4.4 GeV and Additional Structure Near 4.1 GeV in e^+e^- Annihilation*, *Phys. Rev. Lett.* **36** (1976) 700.
- [35] P. A. Rapidis et al., *Observation of a Resonance in e^+e^- Annihilation Just Above Charm Threshold*, *Phys. Rev. Lett.* **39** (1977) 526.

- [36] G. S. Abrams et al., *Measurement of the parameters of the $\psi''(3770)$ resonance*, *Phys. Rev.* **D21** (1980) 2716.
- [37] J. Siegrist et al., *Hadron Production by e^+e^- Annihilation at Center-Of-Mass Energies Between 2.6 GeV and 7.8 GeV. Part 1. Total Cross-Section, Multiplicities and Inclusive Momentum Distributions*, *Phys. Rev.* **D26** (1982) 969.
- [38] A. H. Hoang and M. Jamin, *\overline{MS} Charm Mass from Charmonium Sum Rules with Contour Improvement*, *Phys. Lett.* **B594** (2004) 127–134, [[hep-ph/0403083](#)].
- [39] K. G. Chetyrkin et al., *Charm and Bottom Quark Masses: an Update*, *Phys. Rev.* **D80** (2009) 074010, [[arXiv:0907.2110](#)].
- [40] J. H. Kuhn, M. Steinhauser, and C. Sturm, *Heavy quark masses from sum rules in four-loop approximation*, *Nucl. Phys.* **B778** (2007) 192–215, [[hep-ph/0702103](#)].
- [41] **Particle Data Group** Collaboration, W. M. Yao et al., *Review of particle physics*, *J. Phys.* **G33** (2006) 1–1232.
- [42] **HPQCD** Collaboration, I. Allison et al., *High-Precision Charm-Quark Mass from Current-Current Correlators in Lattice and Continuum QCD*, *Phys. Rev.* **D78** (2008) 054513, [[arXiv:0805.2999](#)].
- [43] C. McNeile, C. T. H. Davies, E. Follana, K. Hornbostel, and G. P. Lepage, *High-Precision c and b Masses, and QCD Coupling from Current-Current Correlators in Lattice and Continuum QCD*, *Phys. Rev.* **D82** (2010) 034512, [[arXiv:1004.4285](#)].
- [44] S. Bodenstein, J. Bordes, C. Dominguez, J. Penarrocha, and K. Schilcher, *QCD sum rule determination of the charm-quark mass*, *Phys. Rev.* **D83** (2011) 074014, [[arXiv:1102.3835](#)].
- [45] J. Penarrocha and K. Schilcher, *QCD Duality and the Mass of the Charm Quark*, *Phys. Lett.* **B515** (2001) 291–296, [[hep-ph/0105222](#)].
- [46] G. D’Agostini, *On the use of the covariance matrix to fit correlated data*, *Nucl. Instrum. Meth.* **A346** (1994) 306–311.
- [47] T. Takeuchi, *The Status of the determination of $\alpha(m_Z)$ and $\alpha_s(m_Z)$* , *Prog. Theor. Phys. Suppl.* **123** (1996) 247–264, [[hep-ph/9603415](#)].
- [48] K. Hagiwara, A. D. Martin, D. Nomura, and T. Teubner, *Predictions for $g - 2$ of the muon and $\alpha_{QED}(M_Z^2)$* , *Phys. Rev.* **D69** (2004) 093003, [[hep-ph/0312250](#)].
- [49] F. Le Diberder and A. Pich, *The perturbative QCD prediction to R_τ revisited*, *Phys. Lett.* **B286** (1992) 147–152.
- [50] A. A. Pivovarov, *Renormalization group analysis of the tau-lepton decay within QCD*, *Z. Phys.* **C53** (1992) 461–464, [[hep-ph/0302003](#)].
- [51] E. Braaten, S. Narison, and A. Pich, *QCD analysis of the tau hadronic width*, *Nucl. Phys.* **B373** (1992) 581–612.
- [52] S. Narison and A. Pich, *QCD Formulation of the tau Decay and Determination of Λ_{MS}* , *Phys. Lett.* **B211** (1988) 183.
- [53] E. Braaten, *The Perturbative QCD Corrections to the Ratio R for tau Decay*, *Phys. Rev.* **D39** (1989) 1458.
- [54] E. Braaten, *QCD Predictions for the Decay of the tau Lepton*, *Phys. Rev. Lett.* **60** (1988) 1606–1609.

- [55] P. A. Baikov, V. A. Ilyin, and V. A. Smirnov, *Gluon condensate fit from the two loop correction to the coefficient function*, *Phys. Atom. Nucl.* **56** (1993) 1527–1530.
- [56] K. Chetyrkin, J. Kuhn, A. Maier, P. Maierhofer, P. Marquard, et al., *Precise Charm- and Bottom-Quark Masses: Theoretical and Experimental Uncertainties*, *Theor.Math.Phys.* **170** (2012) 217–228, [[arXiv:1010.6157](#)].
- [57] S. Narison and R. Tarrach, *Higher dimension renormalization group invariant vacuum condensates in Quantum Chromodynamics*, *Phys. Lett.* **B125** (1983) 217.
- [58] B. L. Ioffe, *QCD at low energies*, *Prog. Part. Nucl. Phys.* **56** (2006) 232–277, [[hep-ph/0502148](#)].
- [59] A. H. Hoang, *Bottom Quark Mass from Upsilon Mesons*, *Phys. Rev.* **D59** (1999) 014039, [[hep-ph/9803454](#)].
- [60] O. V. Tarasov, A. A. Vladimirov, and A. Y. Zharkov, *The Gell-Mann-Low Function of QCD in the Three Loop Approximation*, *Phys. Lett.* **B93** (1980) 429–432.
- [61] S. A. Larin and J. A. M. Vermaseren, *The Three loop QCD Beta function and anomalous dimensions*, *Phys. Lett.* **B303** (1993) 334–336, [[hep-ph/9302208](#)].
- [62] T. van Ritbergen, J. A. M. Vermaseren, and S. A. Larin, *The four-loop beta function in quantum chromodynamics*, *Phys. Lett.* **B400** (1997) 379–384, [[hep-ph/9701390](#)].
- [63] K. G. Chetyrkin, *Quark mass anomalous dimension to $O(\alpha_s^4)$* , *Phys. Lett.* **B404** (1997) 161–165, [[hep-ph/9703278](#)].
- [64] J. A. M. Vermaseren, S. A. Larin, and T. van Ritbergen, *The 4-loop quark mass anomalous dimension and the invariant quark mass*, *Phys. Lett.* **B405** (1997) 327–333, [[hep-ph/9703284](#)].
- [65] **Particle Data Group** Collaboration, J. Beringer et al., *Review of Particle Physics (RPP)*, *Phys.Rev.* **D86** (2012) 010001.
- [66] D. Nomura and T. Teubner, *private communication*.
- [67] S. Bodenstein, J. Bordes, C. A. Dominguez, J. Penarrocha, and K. Schilcher, *Charm-quark mass from weighted finite energy QCD sum rules*, *Phys. Rev.* **D82** (2010) 114013, [[arXiv:1009.4325](#)].
- [68] S. Narison, *Gluon condensates and c , b quark masses from quarkonia ratios of moments*, *Phys. Lett.* **B693** (2010) 559–566, [[arXiv:1004.5333](#)].
- [69] K. Chetyrkin, A. Kataev, and F. Tkachov, *Higher Order Corrections to $\sigma_t(e^+e^- \rightarrow \text{Hadrons})$ in Quantum Chromodynamics*, *Phys.Lett.* **B85** (1979) 277.
- [70] M. Dine and J. Sapirstein, *Higher Order QCD Corrections in e^+e^- Annihilation*, *Phys.Rev.Lett.* **43** (1979) 668.
- [71] W. Celmaster and R. J. Gonsalves, *An Analytic Calculation of Higher Order Quantum Chromodynamic Corrections in e^+e^- Annihilation*, *Phys.Rev.Lett.* **44** (1980) 560.
- [72] S. Gorishnii, A. Kataev, and S. Larin, *Next-To-Leading $O(\alpha_s^3)$ QCD Correction to $\sigma_t(e^+e^- \rightarrow \text{Hadrons})$: Analytical Calculation and Estimation of the Parameter Lambda (MS)*, *Phys.Lett.* **B212** (1988) 238–244.
- [73] S. Gorishnii, A. Kataev, and S. Larin, *Correction $O(\alpha_s^3)$ to $\sigma_{\text{tot}}(e^+e^- \rightarrow \text{hadrons})$ in quantum chromodynamics*, *JETP Lett.* **53** (1991) 127–131.

- [74] W. Bernreuther and W. Wetzel, *Order α_s^2 Massive Quark Contribution to the Vacuum Polarization of Massless Quarks*, *Z.Phys.* **C11** (1981) 113.
- [75] S. Gorishnii, A. Kataev, and S. Larin, *Three Loop Corrections of Order $O(M^2)$ to the Correlator of Electromagnetic Quark Currents*, *Nuovo Cim.* **A92** (1986) 119–131.
- [76] K. Chetyrkin and A. Kwiatkowski, *Mass corrections to the tau decay rate*, *Z.Phys.* **C59** (1993) 525–532, [[hep-ph/9805232](#)].
- [77] K. Chetyrkin and J. H. Kuhn, *Quartic mass corrections to R_{had}* , *Nucl.Phys.* **B432** (1994) 337–350, [[hep-ph/9406299](#)].
- [78] K. Chetyrkin, R. Harlander, and J. H. Kuhn, *Quartic mass corrections to R_{had} at order α_s^3* , *Nucl.Phys.* **B586** (2000) 56–72, [[hep-ph/0005139](#)].
- [79] A. H. Hoang and T. Teubner, *Analytic calculation of two loop corrections to heavy quark pair production vertices induced by light quarks*, *Nucl. Phys.* **B519** (1998) 285–328, [[hep-ph/9707496](#)].
- [80] A. H. Hoang, M. Jezabek, J. H. Kuhn, and T. Teubner, *Radiation of heavy quarks*, *Phys. Lett.* **B338** (1994) 330–335, [[hep-ph/9407338](#)].
- [81] **Particle Data Group** Collaboration, K. Nakamura et al., *Review of particle physics*, *J. Phys.* **G37** (2010) 075021.
- [82] T. Gehrmann, G. Luisoni, and P. F. Monni, *Power corrections in the dispersive model for a determination of the strong coupling constant from the thrust distribution*, *Eur.Phys.J.* **C73** (2013) 2265, [[arXiv:1210.6945](#)].
- [83] R. Abbate, M. Fickinger, A. H. Hoang, V. Mateu, and I. W. Stewart, *Precision Thrust Cumulant Moments at N^3LL* , *Phys.Rev.* **D86** (2012) 094002, [[arXiv:1204.5746](#)].
- [84] R. Abbate, M. Fickinger, A. H. Hoang, V. Mateu, and I. W. Stewart, *Thrust at N^3LL with Power Corrections and a Precision Global Fit for $\alpha_s(m_Z)$* , *Phys. Rev.* **D83** (2011) 074021, [[arXiv:1006.3080](#)].
- [85] R. Frederix, S. Frixione, K. Melnikov, and G. Zanderighi, *NLO QCD corrections to five-jet production at LEP and the extraction of $\alpha_s(M_Z)$* , *JHEP* **11** (2010) 050, [[arXiv:1008.5313](#)].
- [86] T. Gehrmann, M. Jaquier, and G. Luisoni, *Hadronization effects in event shape moments*, *Eur. Phys. J.* **C67** (2010) 57–72, [[arXiv:0911.2422](#)].
- [87] J. Blumlein, H. Bottcher, and A. Guffanti, *Non-singlet QCD analysis of deep inelastic world data at $O(\alpha_s^3)$* , *Nucl. Phys.* **B774** (2007) 182–207, [[hep-ph/0607200](#)].
- [88] J. Blumlein and H. Bottcher, *QCD Analysis of Polarized Deep Inelastic Scattering Data*, *Nucl. Phys.* **B841** (2010) 205–230, [[arXiv:1005.3113](#)].
- [89] S. Bethke, *The 2009 World Average of $\alpha_s(M_Z)$* , *Eur. Phys. J.* **C64** (2009) 689–703, [[arXiv:0908.1135](#)].
- [90] S. Alekhin, J. Blümlein, K. Daum, K. Lipka, and S. Moch, *Precise charm-quark mass from deep-inelastic scattering*, *Phys.Lett.* **B720** (2013) 172–176, [[arXiv:1212.2355](#)].
- [91] S. Alekhin, K. Daum, K. Lipka, and S. Moch, *Determination of the charm-quark mass in the $\overline{\text{MS}}$ scheme using charm production data from deep inelastic scattering at HERA*, *Phys.Lett.* **B718** (2012) 550–557, [[arXiv:1209.0436](#)].
- [92] A. G. Grozin and C. Sturm, *Correlator of heavy-quark currents at small q^2 in the large- β_0 limit*, *Eur. Phys. J.* **C40** (2005) 157–164, [[hep-ph/0412040](#)].

- [93] J. Portoles and P. Ruiz-Femenia, *On the massless contributions to the vacuum polarization of heavy quarks*, *J.Phys.* **G29** (2003) 349–356, [[hep-ph/0107324](#)].
- [94] J. Portoles and P. Ruiz-Femenia, *New contributions to heavy quark sum rules*, *Eur.Phys.J.* **C24** (2002) 439–446, [[hep-ph/0202114](#)].